SOL-GEL PREPARED NIOBIUM OXIDE AND SILICON OXIDE COATINGS ON 316L STAINLESS STEEL FOR BIOMEDICAL APPLICATIONS

BY

DIMPLE PRADHAN

A THESIS

SUBMITTED TO THE FACULTY OF

ALFRED UNIVERSITY

IN PARTIAL FULFILLMENT OF THE REQUIREMENTS
FOR THE DEGREE OF

DOCTOR OF PHILOSOPHY

IN

MATERIALS SCIENCE AND ENGINEERING

ALFRED, NEW YORK

SEPTEMBER, 2016

SOL-GEL PREPARED NIOBIUM OXIDE AND SILICON OXIDE COATINGS ON 316L STAINLESS STEEL FOR BIOMEDICAL APPLICATIONS

BY

DIMPLE PRADHAN

B.S. NATIONAL INSTITUTE OF TECHNOLOGY, ROURKELA (2009)

M.S. ALFRED UNIVERSITY (2012)

SIGNATURE OF AUTHOR _____

APPROVED BY _____

NATHAN P. MELLOTT, ADVISOR

_____

ANTHONY W. WREN, ADVISORY COMMITTEE

_____

DAVID LIPKE, ADVISORY COMMITTEE

_____

YIQUAN WU, ADVISORY COMMITTEE

_____

CHAIR, ORAL THESIS DEFENSE

ACCEPTED BY _____

ALASTAIR N. CORMACK, INTERIM DEAN
KAZUO INAMORI SCHOOL OF ENGINEERING

ACCEPTED BY _____

NANCY J. EVANGELISTA, ASSOCIATE PROVOST
FOR GRADUATE AND PROFESSIONAL PROGRAMS
ALFRED UNIVERSITY

ACKNOWLEDGMENT

First of all, I would like to express my deepest gratitude to my thesis advisor, Dr Nathan.P.Mellott for his continuous support and guidance. With his constant motivation I have grown from strength to strength in every aspect of my work. Thank you for allowing me the freedom to work my way out and being there as and when needed to provide all possible assistance. I have learnt so much from you and will be carrying in forward with me as I go from here. You are a perfect mentor anyone can ever get.

I would also like to thank Dr Lipke and Dr Wren for your help. A large part of my thesis could not be completed without your invaluable suggestion and timely guidance. Thank you so much Dr Lipke, I felt inspired every time I left your office after our meetings. Thank you Dr Wren, a large part of my interest in biomaterials stems from you.

I would also like to thank Gerald Wynick, Jim Thiebaud and Swavek Zdzieszynski for training me to use the instruments and giving their valuable inputs for my work.

I am also thankful to my best friend Chokchai and Fiona, and my fiance Hrishikesh for supporting me throughout. I also would like to wish my friends Priyatham, Ruhil, Yuxuan and Sahar best of luck for your PhD as well.

Finally, I am thankful to my Baba and Amchung for their unwavering support over these years and I would like to dedicate this work to the memory of my beloved mother Late. Sangay Doma Bhutia who has taught me invaluable lessons for life.

TABLE OF CONTENTS

LIST OF TABLES

Page

Chapter II

Chapter III

Chapter IV

LIST OF FIGURES

Page

Chapter I

Chapter II

Chapter III

Chapter IV

ABSTRACT

Medical implants have become an important component in the preventative and reconstructive treatment of patients for a variety of health problems. However, lack of biocompatibility, failure of implant due to corrosion and risk of postoperative infection pose as major challenges for their clinical applications. In order to counteract the above problems sol gel prepared niobium oxide and silicon oxide coatings were deposited on 316L stainless steel by spin coating. The preliminary work consisted of morphology, structure and composition analyses of these coatings by FESEM, XPS and GIXRD. Bioactivity was determined through (1) the analysis of calcium phosphate formation at the surface of coatings as a function of simulated body fluid (SBF) reaction time, (2) viability of osteoblast cells using MTT assay (3) osteoblast cell adhesion and proliferation using FESEM for coated and uncoated 316L stainless steel. Deposition of calcium phosphate layer was confirmed by EDS and SEM analysis.

Corrosion resistances of coated and uncoated stainless steel were evaluated in three different physiological environments such as SBF (pH 7.4), water (pH 7) and SGF (pH 1.2) for different time periods. The reaction of samples was observed in the form of cracking and peeling of coatings, formation of corrosion product, passivation of metallic substrate. The changes in morphology and surface chemistry with time of immersion were evaluated through FESEM along with XPS analysis. Since electrochemical analysis such as open circuit potential (OCP) and linear polarization resistance (Rp) strongly depended on the surface condition of the metallic implant these measurements were performed on an externally corroded sample without disturbing the surface. The results obtained by LPR could give information about the influence of corrosive media on the metallic implant and instantaneous corrosion rate with time of immersion.

A very large portion of implant related infection is caused by Staphylococcus aureus (S.Aureus). To combat the effect of S.aureus, erythromycin was incorporated into niobium oxide coatings. Two innovative techniques (solution route and incipient wetness impregnation route) were adopted for synthesis of drug containing niobium oxide systems. Varying concentration of (10, 40 and 80mg/ml) erythromycin was incorporated and experiments were conducted to evaluate the release of antibiotic after 3 and 34 hours followed by their efficiency via bacterial viability and adhesion on surface.

CHAPTER I: INTRODUCTION

Metallic implants have been used for various clinical applications such as amalgam in dentistry, stainless steel plates to repair fractured bones, titanium screws to fixate broken bones or coated stainless steel stents to secure blood vessels. The first and foremost requirement for the choice of the implant is its acceptability in human body. The implanted material should not cause any adverse reactions such as hypersensitivity, toxicity and inflammation either immediately after implantation or under post operative conditions[1]. Secondly, in addition to sufficient mechanical strength, the biomaterials should possess high corrosion and wear resistance in the highly corrosive environment of the human body. In such corrosive environments, metal ions such as iron, chromium and nickel from the metal implants are released which can cause powerful allergic and carcinogenic reactions[2]. Hence, implant functionality is compromised by poor corrosion resistance and lack of biocompatibility[3, 4]. Further, the implantation process incurs a complex set of interactions between host and the implant and is often associated with risk of bacterial adhesion and inflammation. These can weaken the immune system and necessitate additional surgeries[5]. One possible solution for problems associated with the application of metallic implant is surface modification. This is achieved by coating the metal implant with appropriate ceramic oxides for improved biocompatibility and corrosion resistance. Biocompatible and corrosion resistant metal oxide coatings with controlled drug delivery profiles could significantly improve the success of metallic implants in the field of medicine.

The objectives of this work were to successfully deposit crack-free and homogeneous niobium and silicon oxide on 316L stainless steel. Investigate the biocompatibility of coatings by SBF testing, cell viability and osteoblast adhesion. Evaluate corrosion resistance of coated and uncoated 316L stainless steel on the basis of the structural and morphological changes with time of immersion in water, SBF and SGF. The structural and morphological changes in samples post immersion were correlated to the linear polarization resistance values. Further, erythromycin in different concentration

was integrated into the coatings by two different routes. Experiments associated with controlled release of drugs in biological fluids and bacterial studies were performed.

1. Choice of implant material

Metal alloys as implants are utilized in the repair, augmentation, or replacement of bones, teeth, and joints due to their excellent mechanical properties[4, 6]. Although metal alloys satisfy the mechanical requirements, they are generally bioinert and become encapsulated by fibrous tissue, isolating it from the surrounding bone resulting in the inability to attach to the live bone once implanted. Several titanium alloys specifically, Ti-6Al-4V, Ti-5Al-2.5Fe, and Ti-6Al-7Nb and pure grade Ti are known to provide high strength (yield strength =100-896 MPa) and comparatively better corrosion resistance characteristics than 316L stainless steel (SS 316L). However, their extensive use in the economically developing countries is limited by the cost of implants[3,7]. Stainless steel (SS 316L) also offers several benefits such as good mechanical properties relative to those of bone mineral, ease of fabrication along with economical viability which makes it a promising alternative for use as bone plates, screws and artificial joints[3,8]. In SS 316L, a passive surface oxide film consisting of iron and chromium and small amount of molybdenum is formed. However, the film is not stable and its composition changes according to the exposed environment. This causes release of metal ions and affects durability and lifetime of the stainless steel[2, 9]. It has been reported that more than 90% of SS devices fail due to significant pitting and crevice corrosion attack. The severity of attack is said to increase with implantation time[9]. Acid passivation of stainless steel by immersing in acids, such as citric acid, hydrochloric acid, and especially nitric acid, is reported to remove sulfide inclusions and eliminate preferential site of corrosion attacks[10, 11]. Further Cr:Fe ratio increases suggesting chromium enrichment at the surface as a result of acid passivation[7]. One of the possible solutions is coating the surface of stainless steel with metal oxides which can enhance the performance of alloy by imparting biocompatibility and improving the corrosion resistance. Several studies have confirmed that coating of SS 316L with biocompatible oxides such as hydroxyapatite, calcium phosphate, Nb_2O_5, TiO_2 or SiO_2 can also improve its bioactivity and corrosion resistance[6, 9, 12, 13].

2. *Sol gel prepared metal oxide coatings*

The protection of metals by covering the surface with appropriate coatings is a good way to take advantage of mechanical properties while introducing biocompatibility and improving of localized corrosion attacks and leaching problems at the same time. Deposition of biocompatible coatings improved the bonding of the implant with the surrounding tissues[14]. A wide range of coatings have been applied onto metallic substrates ranging from bioactive glasses to hydroxyapatite and oxide coatings[8].

Specifically, niobium and silicon oxides were considered for this study due to excellent corrosion resistance and biocompatibility[15]. Silica was chosen as it is a natural catalyst for hydroxyapatite formation and also have proved to improve corrosion behavior of 316L stainless steel[16]. It has been reported that a coating from aged sols is less effective in corrosion protection than a coating from fresh sols. This is due to growth of silica polymers in aged gel due to condensation reaction which during drying of solvent formed larger and stronger gel network resulting in the formation of a more porous structure with decreased corrosion protection[17]. Niobium oxide films are considered a possible candidate for corrosion resistant biomedical coatings. Inherent porosity of niobium oxide in particular, can induce biologically active bone like apatite layer on the implants[18, 19]. Mechanical studies have confirmed that niobium oxide has excellent adherence to stainless steel substrates[19].

Previous studies have shown that corrosion resistance provided by crystalline sputtered coatings to metallic substrates is affected by inter-columnar space between the film structure and high density of growth related defects such as pores and pinholes which permit corrosion attacks of the substrate. Hence, amorphous coatings can provide better resistance in such situations due to absence of columnar structures [6].

Coatings can be prepared by various techniques such as plasma spraying, sputtering[12, 20], electrochemical deposition[21] and sol gel processing[18, 22]. However, sol-gel technique is preferred over others mainly because of the several advantages it offers such as a simple synthesis process, homogeneous coating, ability to coat complex shapes[17]. Functional coatings can be prepared by changing precursor solutions and modifying thermal treatments[23]. Sol gel coatings have shown excellent chemical stability, oxidation control and enhanced corrosion resistance when deposited on metallic substrates[24]. Sol

gel prepared metal oxides in particular, titania, silica as well as niobium oxide (although less common) deposited on metal alloy-based biomaterials are known to counteract the problems associated with clinical applications of metallic implants[3, 18, 25].

3. Biocompatibility and cytotoxicity of coatings

When a bioactive implant material is placed inside the human body, besides the osteoblast cells, nucleation of bone-like apatite (calcium phosphate layer) is induced on the implant surface. It has been reported that these particles are preferentially deposited along the grooves created during grinding process. Space restrictions induces these particles to fuse together to generate plate like crystals[14, 26]. The speed and morphology of calcium phosphate layer are important in determining early bone-implant integration[27].

The deposition of apatite is reported to be a function of surface roughness, the presence of Si-OH and Nb-OH group at the surface and the structure of the metal oxide coating. The number of -OH groups at the surface decreases with increase in heat treatment temperature. It has been reported that both amorphous and orthorhombic niobium oxide (800^{o}C) on glass shows favorable conditions for apatite nucleation. However, monoclinic niobium oxide (1000^{o}C) does not show any evidence of CaP layer formation. Owing to a comparatively small temperature difference, the number of –OH groups on orthorhombic and monoclinic niobium oxide are nearly same. Hence the disparity in apatite forming ability is attributed to surface charge [28, 29]. It has been reported that apatite formation is induced by negatively charged functional groups. The orthorhombic niobium oxide is reported to be more negatively charge than monoclinic due to conversion of NbO_4 tetrahedral unit in former to NbO_6 octahedral unit in latter. This makes the surface of orthorhombic niobium oxide more favorable for CaP deposition.

Osteoblast cells are known to preferentially proliferate and differentiate to produce bone apatite and collagen on the bioactive apatite layer[14]. Amorphous Nb_2O_5 coatings with smooth surfaces exhibited fastest cell adhesion[30]. However, Eisenbarth et.al have reported excellent biological response on crystalline Nb_2O_5[31]. It is not yet clearly understood the precise parameters that affects the osteoblasts response on a surface. There are indications that surface roughness, hydrophilic nature, composition, wettability and surface free energy might have a role in the cell adhesion response[25, 32, 33].

4. Corrosion in biological environment

The human body is not an environment that one would consider hospitable for an implanted metal alloy: a highly oxygenated saline electrolyte at a pH of around 7.4 and a temperature of 98.6°F (37°C)[34]. Degradation of metal implants in hostile biological environments is associated with localized corrosion attacks and leaching of metal ions. Simulated Gastric Fluid (SGF) was selected for use in this study due to presence of Cl^- ions which can stimulate pitting and crevice corrosion attacks of the implant in the human body[17]. The release of iron, chromium, and nickel ions from the metal alloys and preferentially Fe ions in chloride containing solutions promotes the formation of fibrous tissue and necrosis around implants[17, 23].

When in an aqueous media, the surface of metallic implants can form hydroxides or oxides, producing a local change in the pH. Furthermore, immediately after implantation, the alloys are surrounded by fibrin and chloride ions, decreasing the local pH, possibly leading to the acceleration of the corrosion process. The conditions inside the human body are reproduced by preparing artificial solutions such as Hartman's solution, sodium chloride (NaCl), Ringer's solution, simulated body fluid (SBF), simulated gastric fluids (SGF) and simulated intestinal fluids (SIF)[7, 8, 12, 17, 35] . These solutions contain salt concentrations similar to actual body fluids. Several alternatives for improving the corrosion resistance of implants have been proposed such as surface passivation, addition of agents which lower molecular oxygen activity at the surface where surface modification by deposition of coatings proves to be one of the most promising options[13, 36]. The stability of coatings is reported to be highly dependent on the structure, chemistry and morphology of coatings as well as chemical composition of fluids. This means a coating may be stable in one solution but may completely fail in another[12].

5. *Electrochemical analysis*

Electrochemical techniques can be used to study many corrosion phenomena and also measure corrosion rates. Typically, experiments are carried out using three electrode cells; the working electrode, the reference electrode and the counter electrodes in contact with electrolyte. The most common choices for electrodes includes Pt wire as auxiliary/counter electrode, Ag/AgCl (+0.197V vs SHE at 25^{o}C) or saturated calomel electrode (+0.241V vs SHE at 25^{o}C) as reference electrode and test sample as a working electrode in a corrosive media.

5.1. Open circuit potential (OCP)

The open circuit potential (OCP) measurement, also known as the corrosion potential, is a summation of the half-cell reaction potentials in the electrolyte of interest and is monitored by measuring the potential vs. a reference electrode using a high impedance voltmeter or electrometer. The potential vs. time response data is collected and stopped when the specimen reaches a steady-state potential with the electrolyte. Steady-state normally occurs within one to three hours of immersion. The corrosion potential is the basis for the linear and potentiodynamic polarization experiments, thus OCP measurements are also taken before these tests. The ASTM G-69 standard practice for testing OCP is followed.

When a specimen is immersed in a corrosive medium it assumes a potential value relative to a reference electrode. The input impedance of reference electrode is ~ $10^{12}\Omega$ *(CH instruments, model 660)* so that for a potential drop of 1 V, an extremely small current of 10^{-14} A will flow in the measuring circuit. This current is too small to interfere with the electrode reactions occurring at the metal/solution interface or to change the electrode potential of the reference electrode. Thus, the electrochemical potential of specimen under study will not be altered during the measurement.

Higher (more positive) potential values (E_{ocp}) are attributed to better corrosion protection. It has been observed that for the same sample, OCP measurements may result in different values depending on the electrolytes. It was reported that the potential of SS 316L in Hartman solution was more positive but showed continuous decrease in OCP value indicating local pitting corrosion while the potential in NaCl was relatively lower[12].

It was reported that OCP values for HA coated SS 316L increased gradually while pristine SS 316L showed a drop in potential demonstrating metal ion dissolution[9].

5.2. Linear polarization resistance (LPR)

The polarization resistance test is a non-destructive electrochemical technique based on a continuous change of an electrode's potential in the vicinity of corrosion potential. Prior to each measurement, open circuit potential (OCP) must be identified with the reference electrode and corrosion performance of the coatings is measured by perturbing the natural open circuit potential (OCP) of the system in both positive and negative direction. Over this small range of potential, the current vs. voltage curve plotted on a linear graph is a straight line. The polarization resistance value, Rp of the corroding electrode is obtained as a slope of the potential versus current density line within the zero current point i=0. The LPR value is designated as *Rp* and is related to corrosion current i_{corr} by,

$$i_{corr} = \frac{B_a B_c}{2.3 R_p (B_a + B_c)} \qquad \text{Equation (1)}$$

The default values for Tafel slopes B_a *and* B_c in the above equation can be considered as 120mV/decade. The corrosion current is related to corrosion rate by,

$$CR = \frac{0.13 i_{corr} (E.W)}{Ad} \qquad \text{Equation (2)}$$

CR= corrosion rate in mpy

E.W. = equivalent weight of the corroding species in g

A = area of corroding surface in cm^2

d = density of the corrosding species in g/cm^2

i_{corr} = corrosion current $\mu A/cm^2$

The R_p value can help access the relative ability of a material to resist corrosion. Considering the test is performed on samples with equal surface area the highest Rp value (lowest corrosion rate) corresponds to higher corrosion resistance.

Although the measurement of LPR appears straightforward various complications could occur while performing the measurements. First, the rate at which the potential is scanned may have a significant effect on the amount of current produced at all values of

potential and if not chosen properly can alter or cause a misinterpretation of the data. Secondly, the distance between the bottom of reference electrode and the working electrode is purposely minimized in most measurements to limit the effect of the solution resistance. The problem from solution resistance has been largely overcome by using a standard three-electrode measurement. This uses separate circuits for the measurement of I and E. The circuit in which the E measurement is made has extremely high input impedance ($10^{12}\Omega$); consequently solution resistance has negligible effect on the value of potential shift applied to the test electrode. Finally, since corrosion reactions take place at the surface of materials, when the surface is changed, due to processing conditions, active corrosion or other reasons, the potential is usually also changed. This can have a strong effect on the polarization curves.

6. Correlation of bioactivity and corrosion resistance

The bioactivity of metal oxides are initially determined by formation of calcium phosphate layer in simulated body fluid(SBF) test[16]. Studies have shown that corrosion resistance in hybrid SiO_2 coatings improved after deposition of apatitic phase which restricts the substrate-electrolyte interaction[8]. The corrosion products formed on 316L stainless steel in body fluids consisted of Cr combined with S and/ Fe combined with P containing Ca and Cl [20]. This can limit the biocompatibility of ceramic oxide and promote degradation in SBF[3]. However, Pauline et.al has reported that HAp growth can prevent electrolyte penetration and acts as an interference layer preventing corrosion[17].

7. Infection during Implantation

Infections associated with implanted medical devices such as joint arthroplasty prostheses have become an increasing concern in orthopedic surgeries[36]. This is due to decreased antibiotic sensitivity and increased requirement by a more numerous ageing population. This can cause bacterial adherence and colonization on the device's surface which leads to biofilm formation.[36,37].

Prosthesis and tissue removal is the most common and typically only option for curing an infection, resulting in serious health, social and economic consequences (increased morbidity, mortality, prolonged hospital stay)[38]. The major source of intra-operative bacterial contamination in joint replacement surgery and other orthopedic

implant surgery is Gram-positive *S.aureus* being most virulent and responsible for approximately 34% of total implant-related infection (Figure 1). These infections can incur not only during/post surgery but anytime during the entire lifetime of the implant[39].

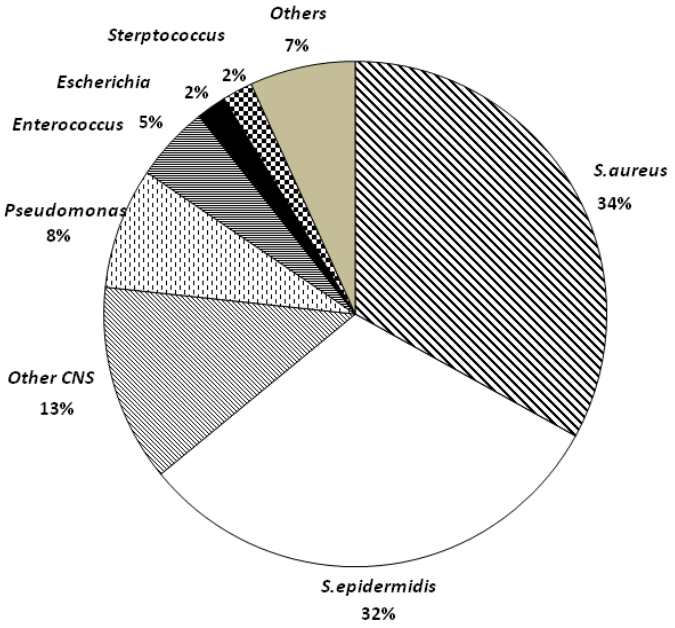

Figure 1. Contribution of different pathogens for implant associated infections

Antibiotics are crucial for prevention of infection during joint replacement implantation procedures. Antibiotics are also significant as infection treatment option in addition to resection of infected tissue and implanted biomaterials. One of the well known antibiotics is erythromycin which is effective against *S.aureus*. It is a macrolide antibiotic which targets the ribosome and inhibits the protein synthesis of Gram positive bacteria[40]. Antibiotics can be delivered to the targeted area either systemically or locally. When antibiotics are administered systemically it creates the risk of damaging other organs. Localized drug delivery is a promising and effective method of sterilizing the implantation site and counteracts bacterial related infections. These reduce the risk of exceeding the toxicity level of drugs and promotes long term controlled release capabilities for different drugs[41].

8. *Sol gel coatings embedded with therapeutic drugs.*

In the past years, drug release systems were associated with polymer matrix. However, the problem of adherence to the metallic substrates and homogeneous distribution of drugs affects the release rate in those samples[42]. In recent years, there has been increased interest in using sol gel technique for possibility of embedding organic compounds for therapeutic and antibacterial uses[26]. Sol-gel processing offers a promising route in controlled release systems due to low processing temperature, ease of controlling pore size and volume. It has been reported that the textural properties of coatings play an important role during the encapsulation process. Pore volume of coatings determines how much of the drug can be released and pore diameter affects the strength of retention of drug since diffusion ate will vary according to the cavity size and increase with pore diameter[26]. Different methods have been tested for successful encapsulation of various compounds such as dipping and drying of implant, immobilization by chemical bonding and by coatings with controlled drug release systems[26]. However, very few studies are dedicated to encapsulation of drugs into coatings.

Two reliable technique for drug encapsulation in coating system are 1) solution route, a one pot sol gel approach in which a desired concentrations of drugs to be mixed into the sols before coating[43] and 2) incipient wetness impregnation route in which the carrier coating is immersed in a drug containing solution and drug is embedded into the matrix by capillary action[44]. In the first process solvent to precursor ratio and water content plays an important role for varying the textural properties of the coating. This process calls for room temperature processing of sol gel coatings as the drugs have very low evaporation temperature and heat treatment tends to densify the system and remove pores[45]. Drugs can be loaded by an incipient wet impregnation method can have the coatings calcined at a desired temperature before the embedment process. Amorphous silica coatings have been reported to encapsulate antiseptic drug by dissolved in ethanol[46]. In recent years, controlled release of vancomycin from silica coated titanium alloys has been reported[43].

9. *Drug release experiments*

Drug release from coatings can be tested by soaking the samples in simulated physiological fluids, alcohol or deionized water for different time periods. Some studies

have reported to allow solution to be stirred during the soaking period[46]. Certain volume of sample can be withdrawn after each time series and evaluated for drug release. The release of drugs in medical fluids tends to lower the pH of SBF (pH 7.4) and SIF (pH 7.4) to 6.6 to 7.2 respectively. This can sometimes restrict further dissolution of drugs affecting its release rate[42]. The release of drugs can be dependent on local pH, solvent used in loading process, interaction between the drug and coatings, porosity of system[46]. The concentration of drug released can be measured using UV-Vis spectroscopy.

10. Antibacterial study

The adherence of bacteria onto device surface is followed by colonization and formation of biofilm. The biofilm acts as a protective covering limiting the effect of antibiotic therapy. Hence, drug incorporated coatings should be able to protect against both bacterial adhesion and biofilm formation. There are various testing methods for antibacterial study such as agar diffusion method which allows the measurement of inhibition zones, broth dilution method is a micro dilution technique where visible bacterial growth is evidenced by turbidity, bactericidal test (spread test) for observation of bacterial colonies on agar plate after different time periods, fluorescent staining of adherent bacteria etc [47-49]. The antibacterial studies are analyzed using SEM, fluorimeter, UV-Vis spectroscopy, plate reader[36].

References

1. Manivasagam G, Dhinasekaran D and Rajamanickam A. Biomedical implants: Corrosion and its prevention-a review. *Recent Pat. .Corros. Sci*. 2010; 2: 40-54.
2. Feng K, Li Z, Cai X and Chu PK. Corrosion behavior and electrical conductivity of niobium implanted 316L stainless steel used as bipolar plates in polymer electrolyte membrane fuel cells. *Surf. Coat. Technol*. 2010; 205: 85-91.
3. Ramírez G, Rodil SE, Arzate H, Muhl S and Olaya JJ. Niobium based coatings for dental implants. *Appl. Surf. Sci*. 2011; 257: 2555-9.
4. Olivares-Navarrete R, Olaya JJ, Ramírez C and Rodil SE. Biocompatibility of Niobium Coatings. *Coatings*. 2011; 1: 72-87.
5. Stigter M, Bezemer J, de Groot K and Layrolle P. Incorporation of different antibiotics into carbonated hydroxyapatite coatings on titanium implants, release and antibiotic efficacy. *J. Controlled Release*. 2004; 99: 127-37.
6. Ramírez G, Rodil SE, Muhl S, et al. Amorphous niobium oxide thin films. *J. Non-Cryst Solids*. 2010; 356: 2714-21.
7. Bidhendi ARH and Pouranvari M. Corrosion study of metallic biomaterials in simulated body fluid. *Metalurgija*. 2011; 17: 13-22.
8. Garcia C, Cere S and Duran A. Bioactive coatings prepared by sol–gel on stainless steel 316L. *J. Non-Cryst. Solids*. 2004; 348: 218-24.
9. Chew K-K, Zein SHS and Ahmad AL. The corrosion scenario in human body: Stainless steel 316L orthopaedic implants. *Natural Science*. 2012; 4.
10. Rojas P and Rodil S. Corrosion Behaviour of Amorphous Niobium Oxide Coatings. *Int. J. Electrochem.Sci*. 2012; 7.
11. Metroke TL, Parkhill RL and Knobbe ET. Passivation of metal alloys using sol–gel-derived materials—a review. *Prog. Org .Coat*. 2001; 41: 233-8.
12. Han Y, Chen D, Sun J, Zhang Y and Xu K. UV-enhanced bioactivity and cell response of micro-arc oxidized titania coatings. *Acta Biomater*. 2008; 4: 1518-29.
13. Nascimento WJ, Bonadio TGM, Freitas VF, Weinand WR, Baesso ML and Lima WM. Nanostructured Nb2O5–natural hydroxyapatite formed by the mechanical alloying method: A bulk composite. *Mater. Chem. and Phys*. 2011; 130: 84-9.
14. Ballarre J, Manjubala I, Schreiner WH, Orellano JC, Fratzl P and Ceré S. Improving the osteointegration and bone–implant interface by incorporation of bioactive particles in sol–gel coatings of stainless steel implants. *Acta Biomater*. 2010; 6: 1601-9.
15. Hosseinalipour S, Ershad-Langroudi A, Hayati AN and Nabizade-Haghighi A. Characterization of sol–gel coated 316L stainless steel for biomedical applications. *Prog. Org. Coat*. 2010; 67: 371-4.
16. Nagarajan S, Raman V and Rajendran N. Synthesis and electrochemical characterization of porous niobium oxide coated 316L SS for orthopedic applications. *Mater. Chem. Phys*. 2010; 119: 363-6.
17. Pauline SA and Rajendran N. Biomimetic novel nanoporous niobium oxide coating for orthopaedic applications. *Appl. Surf. Sci.* 2014; 290: 448-57.
18. Özer N, Chen D-G and Lampert CM. Preparation and properties of spin-coated Nb2O5 films by the sol-gel process for electrochromic applications. *Thin Solid Films*. 1996; 277: 162-8.
19. Gopi D, Ramya S, Rajeswari D and Kavitha L. Corrosion protection performance of porous strontium hydroxyapatite coating on polypyrrole coated 316L stainless steel. *Colloids Surf. B* 2013; 107: 130-6.
20. Hanawa T, Hiromoto S, Yamamoto A, Kuroda D and Asami K. XPS characterization of the surface oxide film of 316L stainless steel samples that were located in quasi-biological environments. *Mate. Trans.* 2002; 43: 3088-92.

21. Gallardo J, Durán A and de Damborenea JJ. Electrochemical and in vitro behaviour of sol–gel coated 316L stainless steel. *Corros. Sci*. 2004; 46: 795-806.
22. Wang D and Bierwagen GP. Sol–gel coatings on metals for corrosion protection. *Prog. Org. Coat*. 2009; 64: 327-38.
23. Ochsenbein A, Chai F, Winter S, Traisnel M, Breme J and Hildebrand HF. Osteoblast responses to different oxide coatings produced by the sol–gel process on titanium substrates. *Acta Biomater*. 2008; 4: 1506-17.
24. Chen X, Nouri A, Li Y, Lin J, Hodgson PD and Wen Ce. Effect of surface roughness of Ti, Zr, and TiZr on apatite precipitation from simulated body fluid. *Biotechnol bioeng*. 2008; 101: 378-87.
25. Campbell AA. Bioceramics for implant coatings. *Materials today*. 2003; 6: 26-30.
26. Böttcher H. Bioactive Sol- Gel Coatings. *Journal für praktische Chemie*. 2000; 342: 427-36.
27. MIYAZAKI T, KIM H-M, KOKUBO T, OHTSUKI C and NAKAMURA T. Apatite-forming ability of niobium oxide gels in a simulated body fluid. *Nippon seramikkusu kyokai gakujutsu ronbunshi*. 2001; 109: 929-33.
28. Liu X, Xie Y, Ding C and Chu PK. Early apatite deposition and osteoblast growth on plasma- sprayed dicalcium silicate coating. *J. Biomedi. Mater. Res. Part A*. 2005; 74: 356-65.
29. Eisenbarth E, Velten D and Breme J. Biomimetic implant coatings. *Biomolecular engineering*. 2007; 24: 27-32.
30. Eisenbarth E, Velten D, Müller M, Thull R and Breme J. Nanostructured niobium oxide coatings influence osteoblast adhesion. *J. Biomedi. Mater. Res. Part A*. 2006; 79A: 166-75.
31. Rosales-Leal JI, Rodríguez-Valverde MA, Mazzaglia G, et al. Effect of roughness, wettability and morphology of engineered titanium surfaces on osteoblast-like cell adhesion. *Colloids Surf., A* 2010; 365: 222-9.
32. Linez-Bataillon P, Monchau F, Bigerelle M and Hildebrand HF. In vitro MC3T3 osteoblast adhesion with respect to surface roughness of Ti6Al4V substrates. *Biomol. Eng*. 2002; 19: 133-41.
33. Hansen DC. Metal corrosion in the human body: the ultimate bio-corrosion scenario. *The Electrochemical Society Interface*. 2008; 17: 31.
34. Motalebi A, Nasr-Esfahani M, Ali R and Pourriahi M. Improvement of corrosion performance of 316L stainless steel via PVTMS/henna thin film. *Prog. Nat. Sci.: Mater Int*. 2012; 22: 392-400.
35. Shih C-C, Shih C-M, Su Y-Y, Su LHJ, Chang M-S and Lin S-J. Effect of surface oxide properties on corrosion resistance of 316L stainless steel for biomedical applications. *Corros. Sci*. 2004; 46: 427-41.
36. Vasconcelos D, Carvalho J, Mantel M and Vasconcelos W. Corrosion resistance of stainless steel coated with sol–gel silica. *J. Non-Cryst. Solids*. 2000; 273: 135-9.
37. Antoci Jr V, Adams CS, Parvizi J, et al. The inhibition of< i> Staphylococcus epidermidis</i> biofilm formation by vancomycin-modified titanium alloy and implications for the treatment of periprosthetic infection. *Biomaterials*. 2008; 29: 4684-90.
38. Stobie N, Duffy B, McCormack DE, et al. Prevention of< i> Staphylococcus epidermidis</i> biofilm formation using a low-temperature processed silver-doped phenyltriethoxysilane sol–gel coating. *Biomaterials*. 2008; 29: 963-9.
39. Montanaro L, Speziale P, Campoccia D, et al. Scenery of Staphylococcus implant infections in orthopedics. *Future Microbiology*. 2011; 6: 1329-49.
40. Campoccia D, Montanaro L and Arciola CR. The significance of infection related to orthopedic devices and issues of antibiotic resistance. *Biomaterials*. 2006; 27: 2331-9.

41. Bagchi A, MUKHERJEE P and RAHA A. DEVELOPMENT AND VALIDATION OF UV SPECTROPHOTOMETRIC METHOD FOR ESTIMATION OF ERYTHROMYCIN IN BULK DRUG AND PHARMACEUTICAL FORMULATION.
42. Simchi A, Tamjid E, Pishbin F and Boccaccini A. Recent progress in inorganic and composite coatings with bactericidal capability for orthopaedic applications. *Nanomedicine: Nanotechnology, Biology and Medicine*. 2011; 7: 22-39.
43. Xu W, Gao Q, Xu Y, et al. Controllable release of ibuprofen from size-adjustable and surface hydrophobic mesoporous silica spheres. *Powder Technology*. 2009; 191: 13-20.
44. Radin S and Ducheyne P. Controlled release of vancomycin from thin sol–gel films on titanium alloy fracture plate material. *Biomaterials*. 2007; 28: 1721-9.
45. Ghedini E, Signoretto M, Pinna F, Crocellà V, Bertinetti L and Cerrato G. Controlled release of metoprolol tartrate from nanoporous silica matrices. *Microporous Mesoporous Mater*. 2010; 132: 258-67.
46. Bhattacharyya S, Agrawal A, Knabe C and Ducheyne P. Sol–gel silica controlled release thin films for the inhibition of methicillin-resistant< i> Staphylococcus aureus</i>. *Biomaterials*. 2014; 35: 509-17.
47. Verraedt E, Pendela M, Adams E, Hoogmartens J and Martens J. Controlled release of chlorhexidine from amorphous microporous silica. *J. Controlled Release*. 2010; 142: 47-52.
48. Akgun BA, Wren AW, Durucan C, Towler MR and Mellott NP. Sol–gel derived silver-incorporated titania thin films on glass: bactericidal and photocatalytic activity. *J.Sol-Gel Sci. Technol*. 2011; 59: 228-38.
49. Reller LB, Weinstein M, Jorgensen JH and Ferraro MJ. Antimicrobial susceptibility testing: a review of general principles and contemporary practices. *Clin.l infect. dis.* 2009; 49: 1749-55.
50. Antoci V, Adams CS, Parvizi J, et al. The inhibition of Staphylococcus epidermidis biofilm formation by vancomycin-modified titanium alloy and implications for the treatment of periprosthetic infection. *Biomaterials*. 2008; 29: 4684-90.

CHAPTER II: NIOBIUM AND SILICON OXIDE COATED 316L FOR IMPROVED SURFACE FUNCTIONALITY OF METALLIC BIOMATERIALS

D. Pradhan[1], *L. Placek*[1], *Y. Gong*[1], *A.W. Wren*[1], *N.P. Mellott*[1,2]*

[1]Inamori School of Engineering, Alfred University, Alfred, NY 14803 USA.

[2]Department of Chemical Engineering and Materials Science, Michigan State University, East Lansing, MI 48842

Keywords: Niobium oxide, coatings, 316L, surface characterization

*To whom all correspondence should be addressed.

Nathan P. Mellott
428 S. Shaw Lane
Department of Chemical Engineering and Materials Science
Michigan State University
East Lansing, MI 48824
mellott3@egr.msu.edu
Ph: 607-760-4944

Abstract

Metallic biomedical implants are the material of choice for a wide range of reconstructive treatments. One of the most common metals used for such treatment is a stainless steel referred to as 316L. These implants often meet the need or exceed mechanical requirements. 316L surfaces are often oxidized, forming a protective oxide layer. This results in adequate chemical durability. However, metals are primarily bioinert and seldom form a strong, direct contact to the natural bone. The chemical and biological performance of such implants can be improved and in some cases controlled and predictable by the addition of functional coatings on the surface of the implant prior to surgery. In order to achieve such performance the coating processing – structure - properties must be clearly understood; including reproducible and optimized deposition methods, bioactivity, and both cell attachment and viability.

We introduce a method to reproducibly modify the surface morphology and composition of a 316L surface which is conducive to the deposition of sol-gel based coatings. Furthermore, the sol-gel processing of sub-micron, crack-free, and spatially homogeneous amorphous niobium oxide and silicon oxide coatings is developed and described in detail. This is achieved through the combination of complementary surface sensitive characterization techniques as well as solution analysis. The bioactivity, as well osteoblast cell viability and attachment of niobium oxide coated, silicon oxide coated, and uncoated 316 L surfaces are directly compared.

1. Introduction

Development of implant materials with desired functionality and performance has become essential in the preventative and reconstructive treatment of patients for a variety of health problems. These implants are utilized in the repair, augmentation, or replacement of bones, teeth, and joints. Implant functionality is dependent upon the chemical-, mechanical-, and biological compatibility of the implant material in a given environment[50]. Although metal alloys satisfy and even surpass mechanical and chemical requirements, they are generally bioinert and become encapsulated by fibrous tissue, isolating it from the surrounding bone resulting in the inability to attach to the live bone once implanted [51-53]. Of the various metallic materials used as orthopedic implants, 316L stainless steel is generally preferred for its economic viability, good corrosion resistance and mechanical properties[10,54]. Application of metal oxide coatings on 316L stainless steel surface is an effective method to improve biocompatibility and have a profound effect on the chemical and biological processes which occur at that interface [17].

Coating structure, chemistry and morphology can affect osteoblastic cell adhesion, proliferation, degree of inflammation, and biomineralization[55-57]. It has been proposed that if the properties of an oxide coating were able to be manipulated both controllably and predictably, then a specific bioactivity can be engineered into a coated implant[6].

There are a wide variety of deposition techniques available to coat metal and metal alloy surfaces including chemical vapor deposition, flame pyrolysis, and sol-gel processing [3,6,18,28,58-61] . In particular sol-gel processing is a leading candidate for the preparation of coatings on metals for biomaterial application given sol-gel processing affords the ability to deposit coatings (1) that are extremely pure with little to no contamination, (2) onto irregularly shaped surfaces, and (3) in a scalable, environmentally conscience, and relatively inexpensive manner[17,62]. Sol gel also affords the ability to prepare inorganic, amorphous metal oxide coatings. It has been shown that in many cases amorphous oxides exhibit equivalent and in some cases better performance properties than their crystalline counterparts[6,29,63] . The processing and chemical and biological properties of the coated 316L must be understood clearly. In particular coating adhesion, composition, morphology, homogeneity, and reproducibility is required[3]. Once

a particular coating is processed and characterized it must be tested for specific biological performance. In particular, the bioactivity of a coating can be evaluated through reaction in simulated body fluid (SBF) where specific attention in focused on the deposition of CaP from solution onto the surface[61]. In addition, osteoblast cell attachment and viability is needed to be understood for many biomedical applications[23,30,55,57,64,65].

Metal oxide coatings for metal implants have been studied for years, with silicon oxides and titanium oxides the two most common[28,51,61,66-70]. However there is significant interest and importance in identifying additional oxide coatings, such that chemical and biological properties are optimized and even tunable [71,72]. One relatively new candidate with high potential is niobium oxide based coatings. However, little is known of the processing or properties of this oxide when coated on metallic surfaces or its' bioactivity and biocompatibility[17]. Several studies have been reported in recent years suggesting that niobium oxide coated stainless steel exhibits superior osteoblast cell attachment and proliferation as well as bioactivity when compared to uncoated stainless steel [29,30]. Still, very little is understood regarding the biological or corrosion resistant properties as well as cell attachment and viability.

In this paper we aim to develop a method to reproducibly modify the surface morphology and composition of a 316L surface conducive to the deposition of sol-gel based coatings. Next, we will describe in detail the method we developed to prepare sub-micron, crack-free, and spatially homogeneous amorphous niobium oxide and silicon oxide coatings. This will be achieved through a combination of complementary surface sensitive characterization techniques. Finally, the bioactivity, as well osteoblast cell viability and attachment of niobium oxide coated 316L, silicon oxide coated 316L, and uncoated 316 L surfaces will be compared and contrasted.

2. Materials and Methods

Substrates were 21 mm diameter 316L stainless steel discs (Swagelok, USA) with an as-published elemental composition of (wt%): Cr 18% max, Ni 14% max, Mo 3% max, Mn 2% max, Si 0.75% max, C 0.04% max, S 0.03 % max, Fe 62.18% max. Prior to deposition of coatings each stainless steel disc was prepared by washing with deionized water and polished with 600 and 1200 grit SiC (water for lubrication). Polished samples were then ultrasonically cleaned in acetone for 20 minutes, followed by immersion in a

0.1M HCl aqueous solution for 3 minutes. Finally, each substrate was rinsed with deionized water, then ethanol, and blown dry with nitrogen gas.

The silica sol was synthesized by mixing tetraethylorthosilicate ($Si(OC_2H_5)_4$, Sigma-Aldrich), ethanol (C_2H_5OH, Fischer Scientific), hydrochloric acid (HCl, Fischer Scientific), and water in a 1:11.4:0.01:5.1 molar ratios [REF]. The resultant sol was then magnetically stirred for 72 hours. The niobia sol was synthesized by mixing niobium ethoxide ($Nb_2(OC_2H_5)_{10}$, Sigma-Aldrich), ethanol (C_2H_5OH, Fischer Scientific), and acetic acid (CH_3COOH, Fischer Scientific) in a 0.01:1:1 molar ratios. The resultant sols were magnetically stirred for 20 minutes prior to coating deposition.

All coatings were then prepared through deposition of approximately 6 drops of coating sol onto a clean stainless steel substrate, followed by spin coating at 1500 rpm for 35 sec. Resultant coated substrates were then dried at 130^{o}C for 12hrs followed by calcination at 450^{o}C for 4hrs in air. This resulted in 3 different types of samples; (1) uncoated stainless steel (UC-SS), (2) niobium oxide coated stainless steel (Nb-SS) and (3) silicon oxide coated stainless steel (SI-SS).

3. Materials Characterization

Glancing incidence X-ray diffraction (GIXRD) analysis was performed on UC-SS, Nb-SS, and Si-SS surfaces using a Siemens Kristalloflex Diffractometer. Diffractograms were recorded in the range $10° < 2\theta > 70°$ at a step size 0.05° s^{-1} and a count time of 2s. The angle of incidence for all measurements was 1.0^o. The GIXRD patterns were analyzed using Jade 9 software (Materials Data Inc., USA) and matched with JCPDS files for crystallographic analysis.

UC-SS, Nb-SS, and Si-SS surface microstructure was observed using scanning electron microscopy (SEM). A FEI Quanta 200F SEM was utilized for low resolution imaging (up to 25,000x), while high resolution imaging (up to 150,00x) was performed on a Zeiss Auriga Cross Beam SEM-FIB. The FEI Quanta 200F SEM was operated at a working distance 7.8 mm and an accelerating voltage 20kV. The Zeiss Auriga Cross Beam SEM-FIB was operated at a working distance of 15 mm and an accelerating voltage of 15kV. Energy dispersive spectroscopy (EDS) was utilized to determine qualitatively, the elements (heavier than boron) present within the uppermost 1 to 3 microns of each sample.

The elemental identification and qualitative chemical composition of UC-SS, Nb-SS, and Si-SS surfaces were analyzed using a PHI Quantera Scanning X-ray photoelectron Microprobe (XPS). XPS scans (0-1250 eV) were collected using Al Kα X-rays (monochromatic, beam size=100 μm) at an output power of 25.5 watts, with an electron energy of 1486.6 eV, a step size of ~0.50 eV, a beam dwell time of ~100 ms, and a pass energy of 140 eV. Five different areas (~1x1 mm each) were analyzed on each sample. Peak position was normalized using the C1s peak (284.6 eV). Resultant spectra were analyzed with PHI Multipak V8.0 software.

4. Bioactivity Analysis

UC-SS, Nb-SS, and Si-SS surfaces were reacted in a simulated body fluid (SBF) for 1, 3, 7, 14, and 21 days. SBF, a tris-buffer solution containing with inorganic ion concentration almost equal to those of human plasma was prepared according to the procedure outlined by Kokubo [73,74]. The reagents; NaCl, $NaHCO_3$, KCl, $K_2HPO_4.3H_2O$, $MgCl_2.6H_2O$, $CaCl_2$, Na_2SO_4, were dissolved in 700ml of deionized water using a magnetic stirrer. The solution was maintained at 36.5±0.5^oC and the pH of the solution was adjusted to 7.4 by adding Tris (hydroxymethyl) aminomethane and 1 M-HCl. The surface area to volume ratio of each sample was 1:10. Coated and uncoated substrates were immersed in the resultant SBF solution for 1, 3,7,14 and 21 days and stored in incubator at 37^oC. Post-reaction SBF leachate solutions were collected after each time frame.

Post-reaction, UC-SS, Nb-SS, and Si-SS surface morphology, structure, and composition was analyzed using the above mentioned characterization techniques, at the same time and under the same conditions as the unreacted samples. In addition, ion concentrations (Ca and P) in the leachate solutions were determined using a Spectro Analytical Instruments inductively coupled plasma atomic emission spectroscopy (ICP-AES). Prior to analysis solution extracts of samples reacted for 1, 3, 7, 14 and 21 days in SBF were filtered with Millipore Hydrophobic Teflon filter (0.2 μm pore size) and diluted by a factor of 100 prior analyses. Each measurement was performed four times per individual aliquot in order to determine the mean concentration of each aliquot.

4.1. Cell culture

Cell culture was conducted using osteoblast MC3T3 cell lines. Cells were initially cultured in Hyclone medium 199/EBSS (Thermo Scientific) supplemented with 10% fetal bovine serum (FBS). Cells were maintained on regular feeding in a CO_2 incubator at 37^oC / 5% CO_2 atmosphere / 100% relative humidity. Media was changed every 2 days. At confluence, cells were detached using a trypsin treatment. The cells were centrifuged and re-suspended in a media containing 10% FBS.

4.2. Cell Viability Analysis

The osteoblast cells after culture were seeded onto a 96 well plate at density of 10^4 cells /well and incubated for 24 hrs prior to testing. MTT assay was used to estimate the cell viability and proliferation. 10µl of sterile extracts for UC-SS, Nb-SS, and Si-SS surfaces were collected after immersion in SBF for 1, 3, 7, 14 and 30 days ($n = 3$). These extracts were added into wells containing osteoblast cells in culture medium (1 ml). The prepared well plates were incubated for 24 hrs at 37^oC / 5% CO_2.

The MTT assay was then added in an amount equal to 10% of the culture medium volume/well. The cultures were then re-incubated for a further 4 hrs (37^oC / 5% CO_2). The cultures were removed from the incubator and the resultant formazan crystals were dissolved by adding an amount of MTT Solubilization Solution (10% Triton X-100 in acidic isopropanol (0.1 N HCI) equal to the original culture medium volume. Once the crystals were fully dissolved, the absorbance was measured at a wavelength of 570 nm. Aliquots (100µl) of tissue culture water were used as controls, and cells were assumed to have metabolic activities of 100%.

Cell viability was compared in relation to 1) maturation (1, 3, 7, 14 and 21 days) and 2) UC-SS, Nb-SS, and Si-SS surfaces. One-way analysis of variance (ANOVA) was applied to determine the statistical significance of the differences observed between samples: $p \leq 0.05$ was deemed significant.

4.3. Cellular adhesion

UC-SS, Nb-SS, and Si-SS substrates before as well as after 21 days of reaction in SBF were sterilized by autoclave prior to the biological tests. All samples were places in 6-well culture plates and osteoblast cells after culture were plated at density of 10^4 cells /well and incubated for 48 hrs prior to fixing. The cells were then fixed with 4%

paraformaldehyde for 30 min and then soaked using 1% osmium tetroxide for 1 hour. This was followed by graded ethanol washes. Finally, the samples were immersed in hexamethyldislizane for 5 minutes and desiccated. The samples were gold coated prior to imaging in SEM.

5. Results

5.1. Substrate and Coating Structure, Morphology, and Composition (pre-SBF Reaction)

GIXRD patterns were obtained for unreacted UC-SS, Nb-SS, and Si-SS calcined at 450^{o}C (not shown). Three diffraction peaks at 2θ values of ~ 43.5^{o}, 44.4^{o} and 50.5^{o} were observed for all samples and was determined to be austenite phase [JCPDS 03-065-4899] belonging to 316 L stainless steel substrate. All peaks for all samples are similar in peak position and relative intensity.

A representative SEM image of UC-SS shown in Figure 1a exhibits a granular structure with spherical particles of ~20 – 100 nm sporadically distributed on the granular structure. Both Nb-SS and Si-SS appeared relatively smooth and featureless in comparison to uncoated stainless steel (Figure 1b and 1c). Furthermore, SEM shows no evidence of cracking or microstructural inhomogeneity of either coating. However Nb-SS films did show evidence of slight surface porosity. The diameters of these pores are approximately 100-200nm (Figure 1b). Silicon oxide coatings do not show any microstructure using the SEM up to 75kx (Figure 1c).

Figure 1d-f shows the representative X-ray photoelectron spectra, including peak positions and assignments collected from UC-SS, Nb-SS, and Si-SS, respectively. Results are shown in Table 1 and summarized here. Analysis of the UC-SS surface revealed the presence of Cr, Fe, Mo in addition to C and O. The XPS spectra obtained for the surface of Nb-SS exhibits the presence of O, Nb, and C; while the XPS spectra obtained for Si-SS showed the presence of O, Si, and C. It is worth noting that each of the five spots measured per sample showed identical spectra.

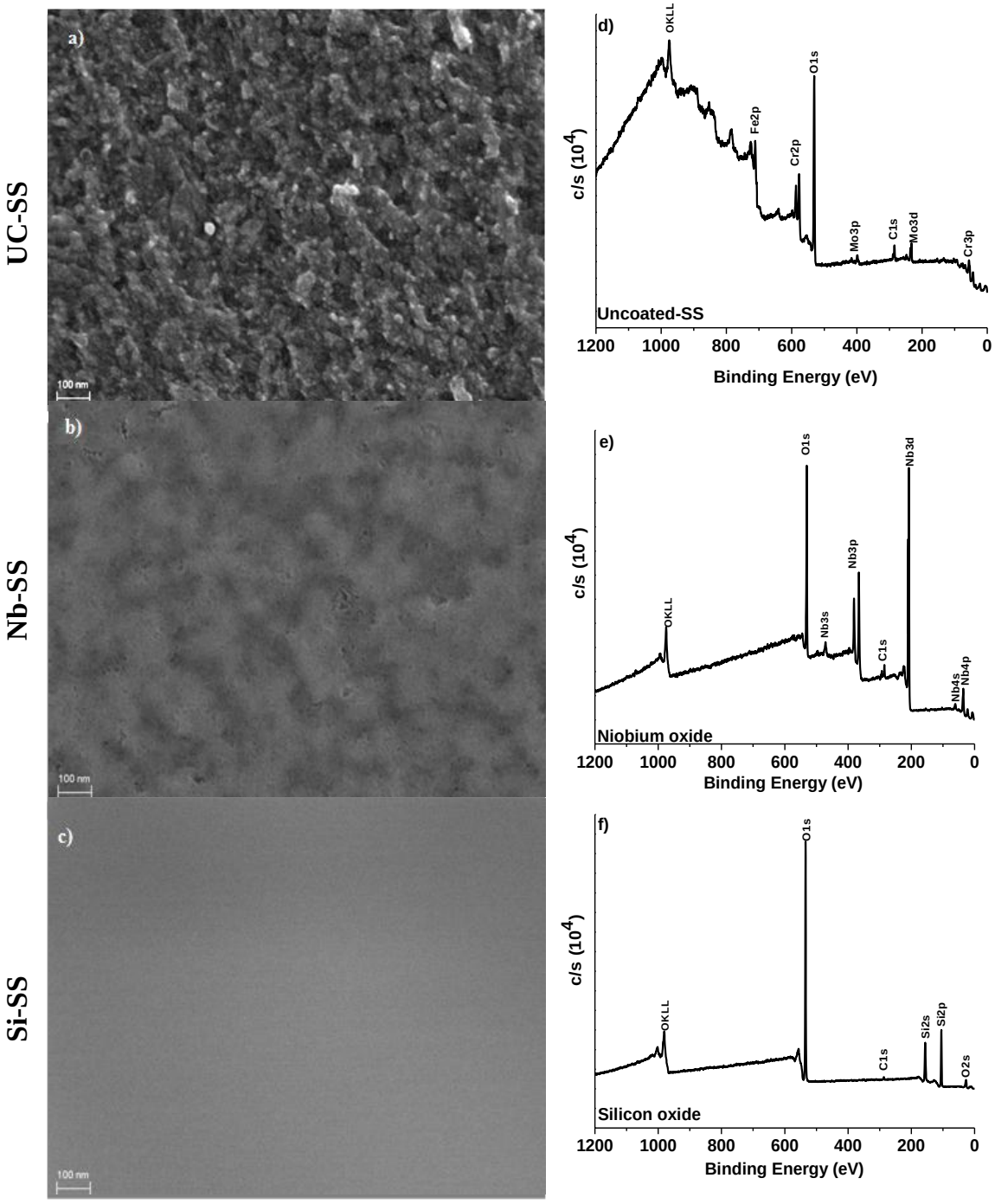

Figure 1. FESEM images (75kx) and corresponding XPS survey scans of a,d) UC-SS, b,e) Nb-SS and c,f) Si-SS.

5.2. Substrate and Coating Structure, Morphology, and Composition (post-SBF Reaction)

GIXRD patterns for UC-SS, Nb-SS, and Si-SS after reaction in SBF for all time periods showed no presence of additional peaks or changes in peak position or shape when compared to unreacted counterparts (results not shown).

After 1 day of reaction in SBF, the entire UC-SS was covered with granular particles of ~50-75 nm (Figure 2a), however no significant changes in microstructure at scales greater than ~100 nm was observed. After reaction for 14 days the granular appearance remains (Figure 2b). EDS analysis suggests that the granular particles are composed of only stainless steel components with no evidence of Ca or P (Figure 2c).

Figure 3a) and 3b) shows the SEM micrographs of NB-SS immersed in SBF for 1 and 14 days, respectively. After 1 day of reaction, the surface appeared irregular and covered with granular particles ~20-50 nm. After reaction for 3, 7, 14 and 21 days, clustered round particles were observed on the coating surface (e.g. 3b). EDS analysis suggests these particles are composed of Ca and P (Figure 3c).

Figure 3d) and 3e) shows the SEM micrograph of Si-SS for 1 and 14 days of immersion in SBF, respectively. The surface morphology after 1 day of immersion in SBF appeared similar to that of the unreacted Si-SS surface, with the exception of the presence of granular particles~50-80 nm present on the surface. After 3, 7, and 14 days clustered round particles of ~100nm are observed on the coating surface with no additional changes in microstructure. After 21 days of SBF reaction, the Si-SS surfaces show significant cracking and exposure of a rough granular surface. EDX analysis performed on the clustered round particles observed on Si-SS reacted for $\geq$ 3 days confirmed the presence of Ca and P at the coating surface (Figure 3f) in addition to coating and substrate elements.

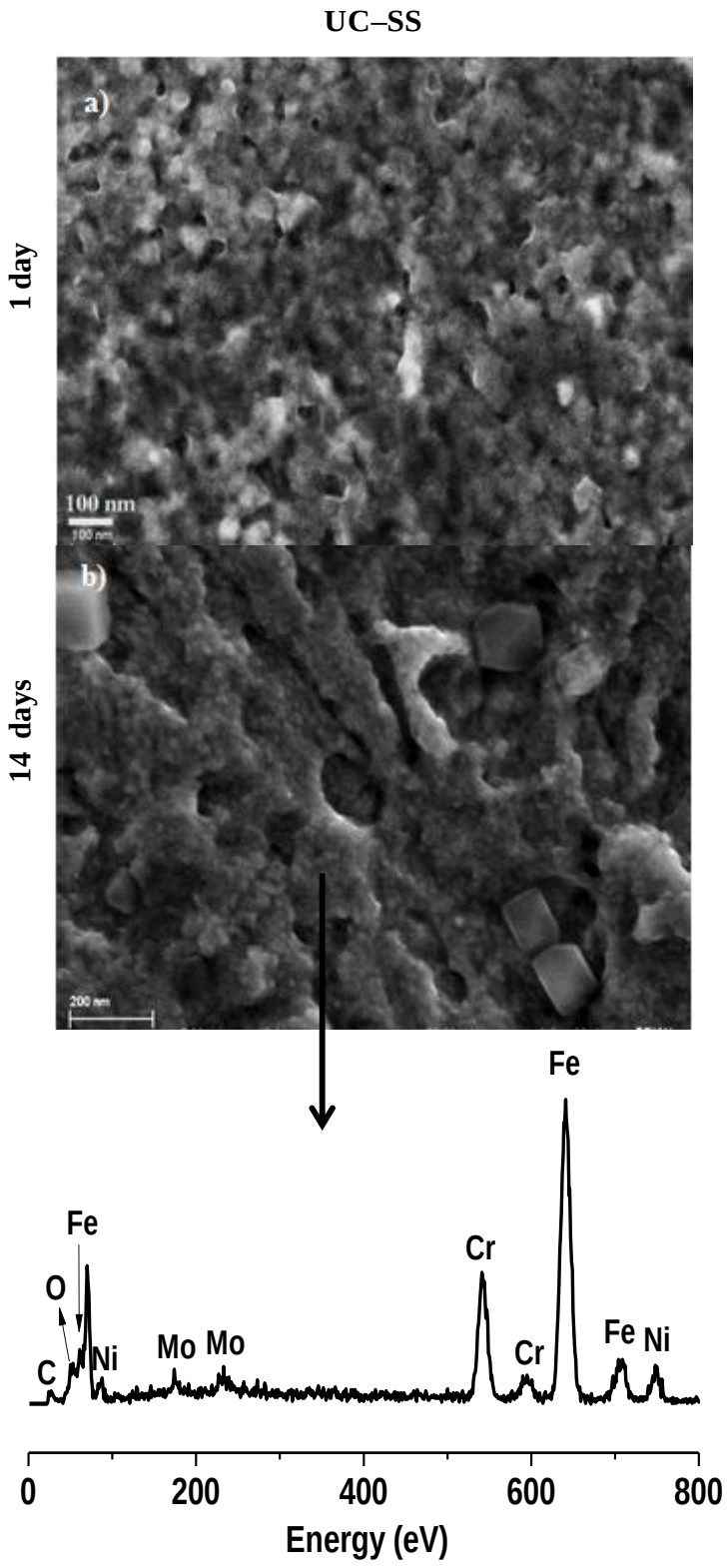

Figure 2. FESEM images of UC-SS after 1 and 14 days immersion in SBF with corresponding EDS spectra shown.

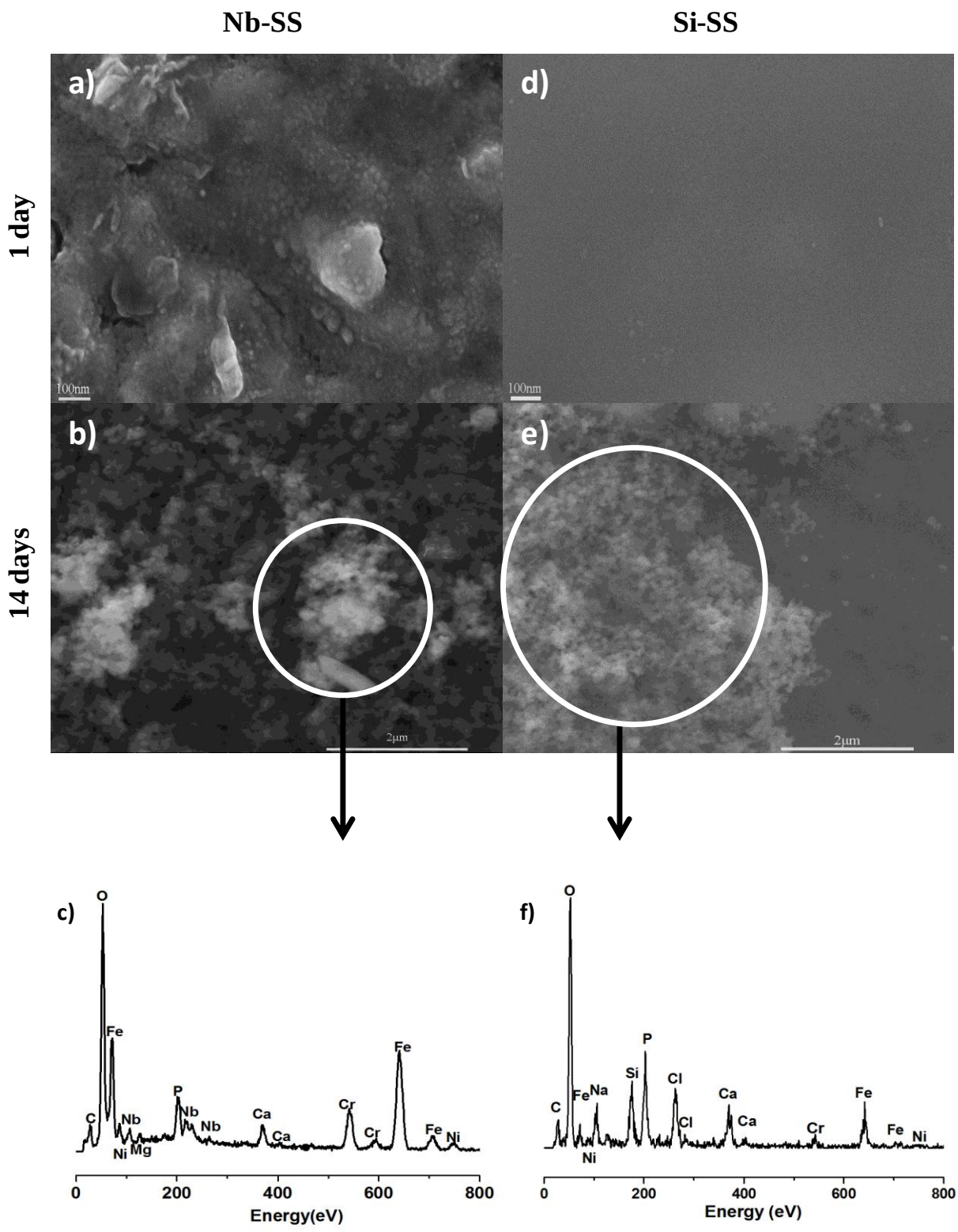

Figure 3. FESEM images for Nb-SS and Si-SS after a) 1 day b) 14 days of immersion in SBF with corresponding EDS spectra shown.

The XPS spectra of UC-SS reacted in SBF for 1, 7 and 14 days showed peaks associated with the substrate itself as well as the presence of Ca and P peaks (Table I). After reaction of the Nb-SS in SBF for 1, 7 and 14 days XPS spectra showed the presence of coating and substrate elements as well as Ca and P. After reaction of Si-SS for 1 day in SBF the surface composition showed only Si and O. After reaction for 7 and 14 days, Si, Ca, P, as well as substrate elements are all present.

Table I. Qualitative surface composition of UC-SS, Nb-SS, and Si-SS after reaction in SBF for different time spans.

Sample	**Reaction Time**	**XPS Identified Element (O and C peaks are present in all samples)**
UC -SS	0	Substrate elements
	1	Substrate elements, Ca, P
	7	Substrate elements, Ca, P
	14	Substrate elements, Ca, P
Nb-SS	0	Nb
	1	Substrate elements, Nb, Ca, P
	7	Substrate elements, Nb Ca, P
	14	Substrate elements, Nb ,Ca, P
Si-SS	0	Si
	1	Si
	7	Substrate elements, Si, Ca, P
	14	Substrate elements, Si, Ca, P

Table II summarizes the concentration of Ca and P in the original SBF solution as well as leachate solutions after reaction of UC-SS, Nb-SS, and Si-SS for up to 21 hours. Following an initial decrease in Ca (30%) and P (13%) concentration after reaction of UN-SS for 1 day the concentration remains relatively constant through 21 days of reaction. With reaction of Nb-SS for 1 day the Ca and P concentrations decrease by 41% and 19% respectively. No further decrease in Ca and P is observed until the reaction time reaches 14 days where a decrease in Ca and P from the original SBF solution reached 74% and 97% respectively. No further decrease in either element is observed after reaction for 21 days. With reaction of Si-SS for 1 day the Ca and P concentrations

decrease by 38% and 16% respectively. No further decrease in Ca and P is observed until the reaction time reaches 7 days where a decrease in Ca and P from the original SBF solution reached 53% and 55% respectively. No further decrease in either element is observed until reaction for 21 days when a decrease in total Ca and P reach 71% and 87% respectively.

Table II. Calcium and phosphorous concentration in SBF leachate solutions as a function of reaction time.

Sample	Time (days)	Ca(ppm)	P(ppm)	% Total Ca Deposited
SBF		100	31	
UC-SS	1	70	27	30
	3	70	27	30
	7	71	28	29
	14	71	28	29
	21	72	28	28
Nb-SS	1	59	25	41
	3	60	26	40
	7	61	26	39
	14	26	1	74
	21	29	3	71
Si-SS	1	62	26	38
	3	63	27	37
	7	47	14	53
	14	48	15	52
	21	29	4	71

5.3. Cell Viability Analysis

The viability of osteoblast cells exposed to UC-SS, Nb-SS, and Si-SS is presented in Figure 4. In comparison to the *Control* cell population, which was assumed to have a metabolic rate of 100%, UC-SS exhibited a decrease in cell viability to 66% after 1 day. However, the statistical variation was not significant for 1-7 days ($p=0.17$). At 14 days, the metabolic rate decreased to 58%, which was significant when statistically compared to the *Control* cell population ($p=0.03$). Finally at 21 days, viability decreased further to 42%, which was significant when statistically compared to the *Control* cell population ($p=0.07$). Nb-SS exhibited an initial metabolic rate increase to 132% followed by a consistent decrease in viability after 3 days. However, statistically the variation was not

significant when compared to *Control* cell population (*p=0.08*). Si-SS exhibited a significant decrease in cell viability at 1 day followed by gradual increase from 3-21 days. At 21 days the metabolic activity recovered to 100%. However the statistically the variation was not significant (*p=0.26*). The effect of maturation between each material at 1, 3, 7, 14 and 21 days were also statistically analyzed.

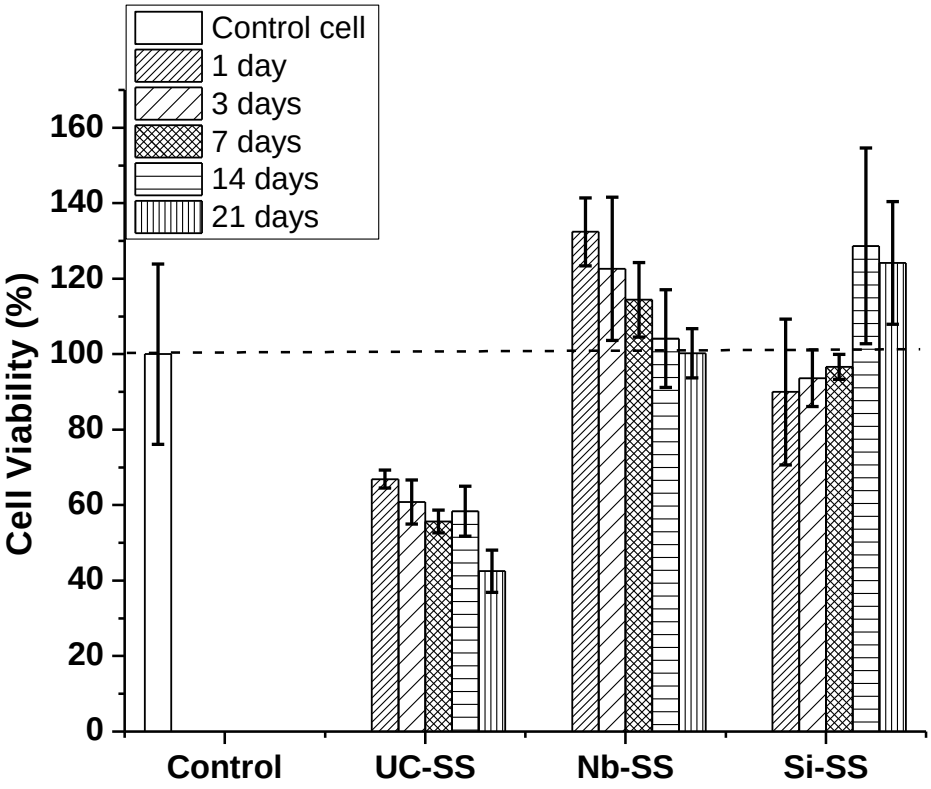

Figure 4. Cell viability analyses for UC-SS, Nb-SS, and Si-SS

5.4. Cellular adhesion

SEM images of the morphology of osteoblast cells on UC-SS, Nb-SS, and Si-SS, after seeding for 48 hours, are shown in Figure 5. Few attached cells are observed on the UC-SS surface. However, the Nb-SS was extensively covered in comparison, with closely packed osteoblast cells exhibiting numerous cytoplasmic extensions and filopodia. The cells attached at the surface were both spread and extended. Si-SS also showed significant osteoblastic cell attachment. However, the numbers of cells attached

were comparatively less than those attached to the Nb-SS surface. The attached cells appeared well spread with cytoplasmic extensions.

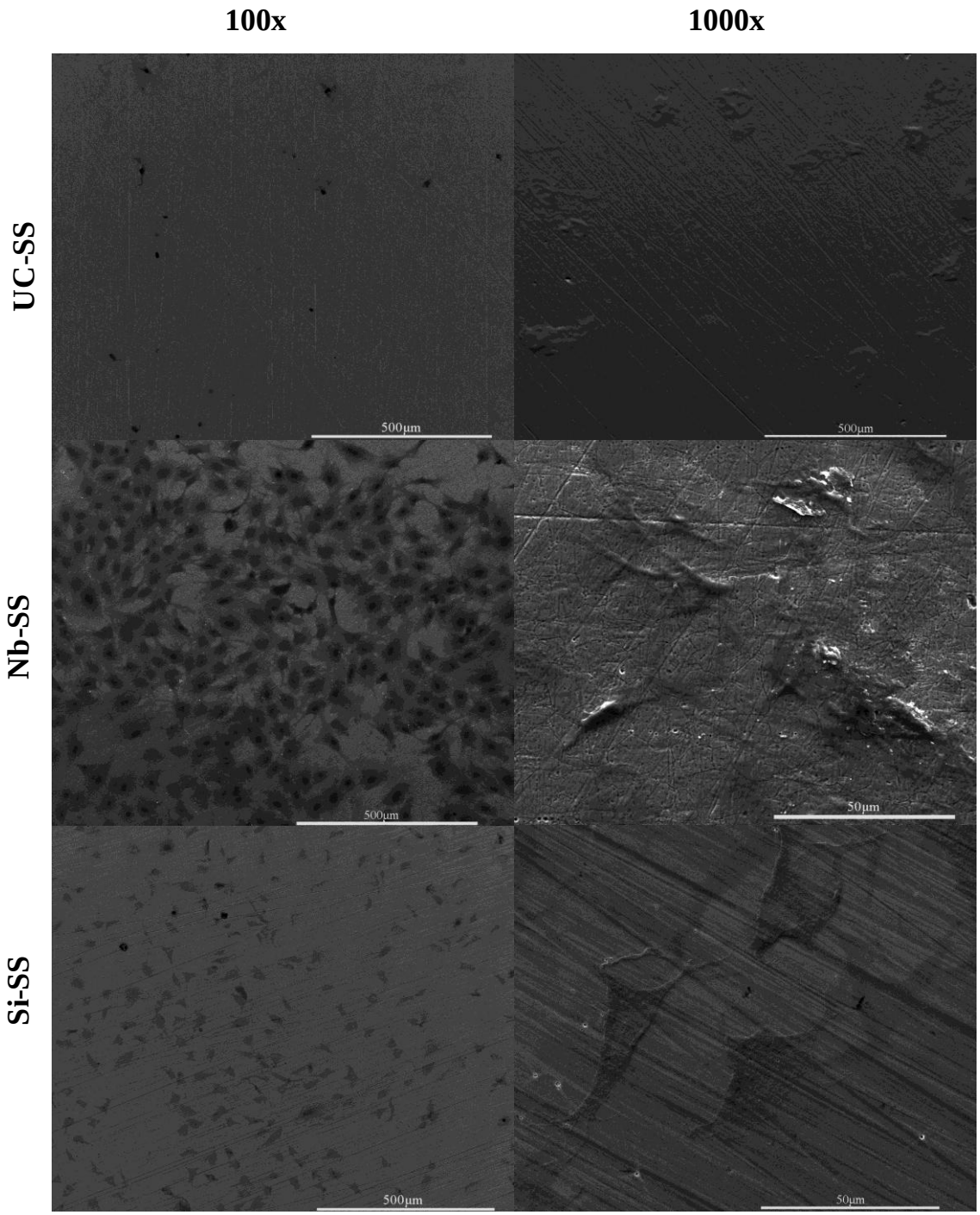

Figure 5. Osteoblast Cell attachments at the surface UC-SS, Nb-SS, and Si-SS.

6. Discussion

6.1. Processing of submicron oxide coatings on surface modified 316L substrates

A method to meticulously and strategically modify the surface composition and morphology was developed in order to promote adhesion of the sol-gel based coatings. The as-received stainless steel disks were first polished on one side to remove any contaminants associated with the packaging and handling of the disks as well as to induce roughening of the substrate. The surface was further roughened through reaction with DI water (polishing lubricant) and HCL (etchant). In addition, these same reactions formed an oxide film on the surface of the surface modified 316L as determined by XPS (Figure 1a). In particular, XPS results show that Ni, Mn, Si, and S are preferential etched. SEM results show that the resultant substrate is homogeneously roughened on the nanometer to micron scale (Figure 1a). Each of the five 100 micron x 100 micron analysis areas of each given sample exhibits identical XPS spectra. Thus, we can conclude that the surface preparation method resulted in a spatially homogenous and reproducible substrate surface composition and morphology. This ensures that the substrate morphology and composition was not a variable when comparing coated and uncoated 316L surfaces throughout this paper.

The first step in the processing of the coating is the development of optically transparent, stable, niobium- and silica-based sols. This was performed through controlled variation of molar ratios and/or mixing methods [75-77]. Silica and niobia sols were both acid catalyzed to promote dense films, post-calcination [75,78]. Niobium and Silicon sol precursor concentrations were designed such that a coating of between 100 and 500 nm would result. This was confirmed via both SEM and Laser Profilometry analysis (not shown).

After spin-coating the resultant sol, the sol-coated-substrate was placed in a drying oven at 130 °C for 12 hours. This ensured cracking was avoided, or at least minimized, as the drying induces release of solvent and water vapor, prior to high temperature densification [78,79]. Finally, dried coatings were calcined at 450 °C for 4 hours in air in order to achieve dense, amorphous oxide coatings well-adhered to the as-prepared 316L substrate. GIXRD of UC-SS, Nb-SS, and Si-SS showed only characteristic peaks of austenitic stainless steel, with no evidence of coating

crystallization (not shown). Spin-coating of sols produced not only reproducible but also spatially homogeneous coatings with respect to thickness and composition; while cracking was avoided. XPS results show that both Nb-SS and Si-SS are crack-free and spatially homogeneous with only expected coating elements, in addition to adventitious carbon. SEM analysis shows homogeneous morphology on the submicron to millimeter scale.

We have developed a method to reproducibly modify the surface morphology and composition of a 316L surface conducive to the deposition of sol-gel based coatings. We also report a method to prepare sub-micron, crack-free, and spatially homogeneous amorphous niobium oxide and silicon oxide coatings on 316L via sol-gel processing. Therefore, can now assess accurately the bioactivity and osteoblast cell response of both coated and uncoated 316L surface and also determine any coating composition effect.

6.2. Bioactivity

Uncoated and coated 316L were soaked in simulated body fluid (SBF) for up to 21 hours to qualitatively determine bioactivity. While there is some question as to whether SBF reactivity effectively models bioactivity, however it is currently a widely accepted method [74,80]. Here, through utilization of various surfaces, near surface, and solution characterization techniques we were able to investigate bioactivity through analysis of the evolution of the surface morphology and crystallinity (SEM and GIXRD), surface composition (XPS), near-surface composition (EDS), as well as the solution chemistry/composition (ICP). In particular it is important to keep in mind how and why these specific techniques are utilized for bioactivity analysis.

Surface morphology (sub-micron and micron scale) was studied through the use of electron microscopy (SEM), with particular focus on coating morphology evolution with time including cracking as well as deposition products from solution (e.g. CaP). GIXRD was useful in the examination of coating crystallinity (or lack-thereof) as well as possible deposited CaP crystallinity. XPS was utilized to determine the surface composition (upper ~8nm) of the substrate or coating. XPS, while only semi-quantitative in nature given the collection parameters, is very sensitive with a conservative estimation of less than 1 atom%. Given this sensitivity as well as its analysis depth were able to investigate CaP deposition as well as cracking of the coating. EDS with a much greater

analysis depth (~1 micron) was utilized to determine the presence of CaP through analysis of features observed while simultaneously imaging with SEM. Finally, ICP analysis of the concentration of Ca in solution afforded us the ability to examine CaP deposition from an angle not typically utilized. With ppm resolution we were able to quantitatively determine the concentration of Ca in solution as a function of reaction time which is directly proportional to the deposition of Ca from solution onto the surface; given both are absent to any reasonable degree in the substrate.

It is clear from SEM analysis that the surface of both coated and uncoated 316L developed a granular morphology on the 50-100 nm scale with reaction in SBF for 1 hour. At durations greater than and equal to 3 days of reaction CaP deposition is observed with SEM/EDS on both coated 316L surfaces, however no evidence of CaP deposition after reaction for 21 days for the uncoated 316Lwas observed. While cracking is observed with reaction in SBF for both types of coatings the Nb-SS exhibited cracking at shorter time frames, while the silicon oxide coating exhibited a much higher degree of cracking and peeling. GIXRD was performed after reaction in SBF to determine the presence of CaP crystallinity. While GIXRD shows no evidence of CaP crystallinity it is worth noting it does not necessarily mean that the CaP observed is not crystalline, given the depth of analysis as well as relatively low expected concentration[28].

The presence of substrate elements observed with XPS after reaction of coated 316L in SBF (Table 1) suggests one of two phenomena occurred; (1) the coating cracked, exposing the substrate or (2) the substrate elements diffused through the coating and is deposited on the surface of the coating. We assume here that it is the former as it unlikely the elements would diffuse through the coating, given the environment of reaction[28,60]. It is also worth noting that XPS showed the presence of Ca and P on the surface of both uncoated and coated 316L after reaction for 1 day. This is consistent with the SEM/EDS results for both coated substrates but not the uncoated 316L surface. However, given the sensitivity of the XPS it is very possible CaP deposition did indeed occur on the UC-SS, however, the morphology of the deposits and/or concentration were below the detection limit of the SEM.

The utilization the ICP to quantify the concentration of Ca in solution as a function of reaction time (Table 2) proved to help lend significant insight into the

development of bioactivity as a function of reaction time for all samples. It was observed that approximately 30% of the Ca available in solution was deposited on the UC-SS substrate after 1 day, however with increased time no additional Ca or P was deposited through 21 days (Table II). This is consistent with SEM/EDS and XPS results. In contrast, after the first 24 hours of reaction approximately 40% of the available Ca in solution was deposited on both coated surfaces, with the increase in Ca deposition with time until ~75% available in solution is deposited at 21 days. These results are also consistent with morphological and compositional analysis of the surface.

A strategic, comprehensive, and complementary set of surface sensitive characterization techniques were utilized in this study, affording the investigation of surface morphology and composition of both coatings and the presence and composition of CaP deposits with reaction in SBF. Assuming the presence and development of CaP is a direct indicator of bioactivity, we show here that both Nb-SS, and Si-SS surfaces exhibit very similar bioactivity and are significantly more bioactive than the uncoated 316L surface. However, it is worth noting that after 21 hours of reaction in SBF the Si-SS coating was significantly cracked, in some cases delaminating, while the Nb-SS exhibited some micro-cracking, it is much more mechanically stable under the conditions. Given the above results we will evaluate the osteoblast cell response as a function of coating presence as well as surface composition.

6.3. Osteoblast Cell Response

The osteoblast cell viability and adhesion was significantly suppressed for the uncoated 316L while both coated samples exhibited good cytocompatibility (Figure 5). The difference in the number of viable cells at the surface of both Nb-SS, and Si-SS coatings were not statistically significant; suggesting the variation in composition of coatings did not affect the growth and metabolic activity of cells. The toxicity of uncoated stainless steel could be attributed to presence of Fe, Cr and Ni ions[81,82].

The Nb-SS surface exhibits more osteoblast cells when compared to both UC-SS and Si-SS coated sample indicating higher cytocompatibility. The osteoblast cells attached on the coated 316L surfaces were well spread and elongated while the cells on the uncoated 316L do not exhibit cytoplasmic extensions and appeared constricted. It is

worth noting as it has been reported that well spread cells are more likely to proliferate over cells that are more constrained [23,83].

These results suggest that osteoblast cell adhesion and viability can be improved with the coating of 316L substrates. Furthermore, it is shown that both the adhesion to and viability of osteoblast cells is higher for the Nb-SS than Si-SS. These results support the notion that niobium oxide coatings exhibit significant potential as a coating material for stainless steel implants [3,4,17,23,30,84] and warrant additional investigation.

7. Conclusions

We have developed a method to reproducibly modify the surface morphology and composition of a 316L surface conducive to the deposition of sol-gel based coatings. We also report a method to prepare sub-micron, crack-free, and spatially homogeneous amorphous Nb-SS and Si-SS via sol-gel processing.

Nb-SS and Si-SS surfaces exhibit higher bioactivity than the uncoated 316L surface. Furthermore we show the bioactivity of the niobium oxide and silicon oxide were very similar, with no clear differences, however, the adhesion of Nb-SS to the surface throughout SBF exposure is clearly higher that the Si-SS. Osteoblast cell adhesion and viability are improved with the coating of 316L substrates. We show that both the adhesion to and viability of osteoblast cells is higher for the niobium oxide coated 316L than the silicon oxide coated 316L.

References

1. Hosseinalipour SM, Ershad-langroudi A, Hayati AN and Nabizade-Haghighi AM. Characterization of sol–gel coated 316L stainless steel for biomedical applications. *Prog Org Coat*. 2010; 67: 371-4.
2. Lin C-M and Yen S-K. Biomimetic growth of apatite on electrolytic TiO2 coatings in simulated body fluid. *Mater. Sci. Eng. C*. 2006; 26: 54-64.
3. Jonášová L, Müller FA, Helebrant A, Strnad J and Greil P. Biomimetic apatite formation on chemically treated titanium. *Biomaterials*. 2004; 25: 1187-94.
4. Xin F, Jian C, Zou J-P, Qian W, Zhou Z-C and Ruan J-M. Bone-like apatite formation on HA/316L stainless steel composite surface in simulated body fluid. *Trans. Nonferrous Met. Soc. China*. 2009; 19: 347-52.
5. Rojas P and Rodil S. Corrosion Behaviour of Amorphous Niobium Oxide Coatings. *Int. J. Electrochem. Sci*. 2012; 7.
6. Chew K-K, Zein SHS and Ahmad AL. The corrosion scenario in human body: Stainless steel 316L orthopaedic implants. 2012.
7. Pauline SA and Rajendran N. Biomimetic novel nanoporous niobium oxide coating for orthopaedic applications. *Appl. Surf. Sci*. 2014; 290: 448-57.
8. Anselme K. Osteoblast adhesion on biomaterials. *Biomaterials*. 2000; 21: 667-81.
9. Eisenbarth E, Linez P, Biehl V, Velten D, Breme J and Hildebrand H. Cell orientation and cytoskeleton organisation on ground titanium surfaces. *Biomol. eng*. 2002; 19: 233-7.
10. Le Guehennec L, Lopez-Heredia M-A, Enkel B, Weiss P, Amouriq Y and Layrolle P. Osteoblastic cell behaviour on different titanium implant surfaces. *Acta Biomater*. 2008; 4: 535-43.
11. Ramírez G, Rodil SE, Muhl S, et al. Amorphous niobium oxide thin films. *J. Non-Cryst. Solids*. 2010; 356: 2714-21.
12. Maček M and Orel B. Electrochromism of sol–gel derived niobium oxide films. *Sol Energy Mater*. 1998; 54: 121-30.
13. Özer N. Optical and electrochemical characteristics of sol-gel deposited tungsten oxide films: a comparison. *Thin Solid Films*. 1997; 304: 310-4.
14. Özer N, Chen D-G and Lampert CM. Preparation and properties of spin-coated Nb2O5 films by the sol-gel process for electrochromic applications. *Thin Solid Films*. 1996; 277: 162-8.
15. Gu Y, Khor K and Cheang P. In vitro studies of plasma-sprayed hydroxyapatite/Ti-6Al-4V composite coatings in simulated body fluid (SBF). *Biomaterials*. 2003; 24: 1603-11.
16. Cui X, Kim H-M, Kawashita M, et al. Preparation of bioactive titania films on titanium metal via anodic oxidation. *Dental materials*. 2009; 25: 80-6.
17. Ramírez G, Rodil SE, Arzate H, Muhl S and Olaya JJ. Niobium based coatings for dental implants. *Appl. Surf. Sci*. 2011; 257: 2555-9.
18. Liu X, Xie Y, Ding C and Chu PK. Early apatite deposition and osteoblast growth on plasma- sprayed dicalcium silicate coating. *J. Biomed. Mater. Res. Part A*. 2005; 74: 356-65.
19. Livage J, Beteille F, Roux C, Chatry M and Davidson P. Sol–gel synthesis of oxide materials. *Acta Mater*. 1998; 46: 743-50.

20. Eisenbarth E, Velten D and Breme J. Biomimetic implant coatings. *Biomol. eng*. 2007; 24: 27-32.
21. Petrov I, Barna P, Hultman L and Greene J. Microstructural evolution during film growth. *J. Vac. Sci. Techno. A*. 2003; 21: S117-S28.
22. Xynos I, Hukkanen M, Batten J, Buttery L, Hench L and Polak J. Bioglass® 45S5 stimulates osteoblast turnover and enhances bone formation in vitro: implications and applications for bone tissue engineering. *Calcif Tissue Int*. 2000; 67: 321-9.
23. Advincula MC, Rahemtulla FG, Advincula RC, Ada ET, Lemons JE and Bellis SL. Osteoblast adhesion and matrix mineralization on sol–gel-derived titanium oxide. *Biomaterials*. 2006; 27: 2201-12.
24. Ochsenbein A, Chai F, Winter S, Traisnel M, Breme J and Hildebrand HF. Osteoblast responses to different oxide coatings produced by the sol–gel process on titanium substrates. *Acta Biomaterialia*. 2008; 4: 1506-17.
25. Eisenbarth E, Velten D, Müller M, Thull R and Breme J. Nanostructured niobium oxide coatings influence osteoblast adhesion. *J. Biomed. Mater. Res. Part A*. 2006; 79A: 166-75.
26. Ghaith E-S, Hayakawa T, Kasuga T and Nogami M. Apatite formation on CO2 laser irradiated titanium oxide films. *Mater. Letters*. 2006; 60: 194-7.
27. Wang X-X, Yan W, Hayakawa S, Tsuru K and Osaka A. Apatite deposition on thermally and anodically oxidized titanium surfaces in a simulated body fluid. *Biomaterials*. 2003; 24: 4631-7.
28. Cheng X-m, Nie B-m and Kumar S. Preparation and bioactivity of SiO2 functional films on titanium by PACVD. *Trans. Nonferrous Met. Soc China*. 2008; 18: 627-30.
29. Rajesh Kumar S, Suresh C, Vasudevan AK, Suja NR, Mukundan P and Warrier KGK. Phase transformation in sol–gel titania containing silica. *Mater Lett*. 1999; 38: 161-6.
30. Vasconcelos DCL, Carvalho JAN, Mantel M and Vasconcelos WL. Corrosion resistance of stainless steel coated with sol–gel silica. *J Non-Cryst Solids*. 2000; 273: 135-9.
31. Rojas P and Rodil S. Corrosion behaviour of amorphous niobium oxide coatings. *Int. J.Electrochem.Sci*. 2012; 7: 1443-58.
32. Ristić M, Popović S and Musić S. Sol–gel synthesis and characterization of Nb2O5 powders. *Mater Lett*. 2004; 58: 2658-63.
33. Maeda H, Kasuga T and Nogami M. Apatite formation on titania–vaterite powders in simulated body fluid. *J Eur Ceram Soc*. 2004; 24: 2125-30.
34. Kokubo T and Takadama H. How useful is SBF in predicting in vivo bone bioactivity? *Biomaterials*. 2006; 27: 2907-15.
35. Fardad M. Catalysts and the structure of SiO2 sol-gel films. *J. Mater. Sci*. 2000; 35: 1835-41.
36. Guglielmi M. Sol-gel coatings on metals. *J. Sol-gel sci. technolo*. 1997; 8: 443-9.
37. Brinker CJ. Sol-gel processing of silica. American Chemical Society, Washington, DC (United States), 1994.
38. Milea C, Bogatu C and Duta A. The influence of parameters in silica sol-gel process. *Bulletin of TheTransilvania University of Brasov*. 2011; 4: 53.

39. Brinker C, Sehgal R, Hietala S, et al. Sol-gel strategies for controlled porosity inorganic materials. *J Membr Sci*. 1994; 94: 85-102.
40. Bohner M and Lemaitre J. Can bioactivity be tested in vitro with SBF solution? *Biomaterials*. 2009; 30: 2175-9.
41. Morais S, Dias N, Sousa J, Fernandes M and Carvalho G. In vitro osteoblastic differentiation of human bone marrow cells in the presence of metal ions. *J Biomed Mater Res*. 1999; 44: 176-90.
42. Mändl S. Increased biocompatibility and bioactivity after energetic PVD surface treatments. *Materials*. 2009; 2: 1341-87.
43. Olmo N, Martí AI, Salinas AJ, Turnay J and Lizarbe MA. Bioactive sol–gel glasses with and without a hydroxycarbonate apatite layer as substrates for osteoblast cell adhesion and proliferation. *Biomaterials*. 2003; 24: 3383-93.
44. Eisenbarth E, Velten D, Müller M, Thull R and Breme J. Biocompatibility of β-stabilizing elements of titanium alloys. *Biomaterials*. 2004; 25: 5705-13.
45. Olivares-Navarrete R, Olaya JJ, Ramírez C and Rodil SE. Biocompatibility of Niobium Coatings. *Coatings*. 2011; 1: 72-87.

CHAPTER III: CORROSION BEHAVIOR OF NIOBIUM OXIDE AND SILICON OXIDE COATED 316L STAINLESS STEEL IN SBF, SGF, AND WATER

D. Pradhan[1], D.W.Lipke[1], A.W.Wren[1], N.P. Mellott[2]*

[1]Inamori School of Engineering, Alfred University, Alfred, NY 14803 USA.

[2]Department of Chemical Engineering and Materials Science, Michigan State University, East Lansing, MI 48842

Keywords: Corrosion, SBF, 316L, surface characterization, Linear polarization resistance

*To whom all correspondence should be addressed.

Nathan P. Mellott
428 S. Shaw Lane
Department of Chemical Engineering and Materials Science
Michigan State University
East Lansing, Mi 48824
mellott3@egr.msu.edu
ph: 607-760-4944

Abstract

Corrosion is one of the major problems affecting the life and service of orthopedic devices made of metals and alloys used as implants in the living body. One of the most common ways to improve corrosion resistance of 316L stainless steel (UC-SS) is by deposition of bioceramic coatings. Amorphous niobium oxide (Nb-SS) and silicon oxide (Si-SS) coated stainless steel specimens were prepared by sol-gel technique. The coatings obtained were crack-free and homogeneous. The coated and uncoated stainless steel was characterized using SEM and XPS for morphological and elemental identification before reaction.

Since corrosion is not only dependent on the choice of material but also on the exposed media, corrosion analyses of UC-SS, Nb-SS and Si-SS were conducted in deionized water, simulated body fluid (SBF) and simulated gastric fluid (SGF). Electrochemical measurements such as open circuit potential (OCP) and linear polarization resistance (Rp) were carried out. The behavior of UC-SS, Nb-SS and Si-SS in different media were characterized using SEM and XPS and the results were correlated with corresponding Rp values to understand the severity of corrosion after specific time period.

1. Introduction

Metallic implants have been frequently employed for many applications such as stents and orthopedic applications. Stainless steel in particular offers good mechanical properties, ease of fabrication and is economically viable compared to Ti alloys[1]. The addition of molybdenum in 316L stainless steel results in improved corrosion resistance especially against pitting in a chloride rich solution[2]. Although 316L stainless steel have excellent mechanical properties and improved corrosion resistance than other alloys of stainless steel, still degradation may occur as corrosion is not only dependent on the properties of implant but is subjected to the environment it is placed in[3,4].

The environment inside the human body consists of a highly oxygenated saline electrolyte at a pH of around 7.4 and a temperature of 98.6°F (37°C) and is subjected to varying changes in pH and temperature owing to differences in local, systemic, environmental, economic and social conditions for each individual[4].Generally, degradation of metal implants in hostile biological environments is associated with leaching of metal ions and presence of corrosive species such as hydrogen ion (H^+), sulfide compounds (S^{2-}), dissolved oxygen, and chloride ion (Cl^-) resulting in the metal surface breakdown and consequent adverse tissue reactions[4,5]. In addition, the presence of proteins, bacteria, and cells inside human body may affect the implant functionality[88]. The presence of Cl^- ions in the human body stimulates pitting and crevice corrosion attacks by preferential Fe ions release promoting the formation of fibrous tissue around the implant[7,8].

In 316L stainless steel, a passive surface oxide film consisting of iron, chromium and a small amount of molybdenum is formed. However, the film is not stable and its composition changes according to the exposed environment. This causes release of metal ions and affects durability and lifetime of the stainless steel[9,10]. It has been reported that more than 90% of SS devices fail due to significant pitting and crevice corrosion attack. The severity of attack is said to increase with implantation period[10]. Immersion of stainless steel in acid such as HCl, HNO_3 or citric acid is reported to eliminate preferential site of corrosion attacks and passivate the surface with Cr-rich layer[11]. Several alternatives for improving the corrosion resistance of implants have been proposed such as surface passivation or addition of agents which lower molecular oxygen

activity at the surface however surface modification by deposition of coatings proved to be one of the most promising options[12,13].

Several studies have shown that coating 316L stainless steel with biocompatible oxides such as hydroxyapatite, calcium phosphate, Nb_2O_5,TiO_2, or SiO_2 can its improve corrosion properties in biological fluids[10,12,14,15]. Silica is known as a natural catalyst for hydroxyapatite formation and is known to improve corrosion behavior of 316L stainless steel[16]. The improved corrosion protection is attributed to better adhesion due to Fe-OH or oxide layer on stainless steel covalently bonding with Si-OH of the sol gel coatings forming dense and uniform Fe-O-Si covalent bond[7]. Vasconcelos et al reported that when SiO_2 is deposited on stainless steel a transpassive intermediate layer composed of Si, O and Fe is formed which improved corrosion resistance[17].

Niobium oxide films are considered a possible candidate for corrosion resistant biomedical coatings. Mechanical studies have confirmed that niobium oxide has excellent adherence to stainless steel substrate[18]. The porosity of niobium oxide provides a pathway for interaction of the electrolyte with metal substrate[3].

Both niobia and silica coatings deposited in this study were amorphous. Some studies have shown that corrosion resistance provided by crystalline sputtered coatings is affected by inter-columnar space and high density of growth related defects such as pores and pinholes which permit corrosion attacks of the substrate. Hence, amorphous coatings can provide better resistance in such situations due to absence of columnar structures[14].

The type of corrosion process occurring is dependent not only on the choice of implant but the dissolution medium[4]. The condition inside human body can be reproduced by preparing artificial solutions such as Hartman's solution, sodium chloride (NaCl), Ringer's solution ,simulated body fluid (SBF), simulated gastric fluids (SGF) and simulated intestinal fluids (SIF)[7,11,15,19,20]. These solutions contain salt concentrations very similar to actual body fluids. For this study, deionized water, SBF and SGF were selected as the corrosion media. Deionized water was chosen as a standard solution and SBF was selected as its composition is similar to human plasma. SGF solution contains Cl^- ions which would help understand the behavior of coated and uncoated 316L stainless steel in these aggressive environments.

When in an aqueous media, metallic surfaces can form hydroxides or oxides, producing a local change in the pH. Furthermore, immediately after implantation, the alloys are surrounded by fibrin and chlorine ions, decreasing the local pH, possibly leading to the acceleration of the corrosion process. In chloride containing solutions, Cl^- ions can get adsorbed on the passivated surface or penetrate the oxide layer through pores or pits. These ions can enter into pits forming concentrated solution of Fe^{2+}, Ni^{2+} and Cr^{3+} chlorides[21]. It has been reported that niobium oxide coatings when immersed in NaCl shows evidence of clear delamination of coatings and strong chemical attack of exposed areas while the film was stable in Hartman solution[3].

There are various electrochemical techniques known for measurement of corrosion such as immersion test, impedance test, Tafel, and linear polarization resistance (LPR). LPR is one of the most common methods which allow monitoring of corrosion rates directly. The values of open circuit potential (OCP) and linear polarization resistance (LPR) are strongly depended on surface conditions.

In this study, the amorphous niobium and silicon oxide coated and uncoated stainless steel samples were first exposed to different corrosive environments namely; deionized water (pH ~7), SBF (pH~7.4) and SGF (pH~1.2) for 1, 3, 7, 14 and 21 days . The first objective was to study the morphological changes at the sample surface and formation of corrosion products using SEM and elemental identification using XPS scans. Secondly, electrochemical measurement using OCP and LPR was performed without disturbing the surface layers of exposed samples. This was done to correlate observations by SEM and XPS with electrochemical data to understand the severity of corrosion and variation in corrosion rate over different time periods.

2. Materials and Methods

2.1. Preparation of substrate

Circular 316L stainless steel substrates (21 mm diameter, Swagelok, USA) with an elemental composition of (wt%): Cr 18% max, Ni 14% max, Mo 3% max, Mn 2% max, Si 0.75% max, C 0.04% max, S 0.03 % max, Fe 62.18% max were polished with 600 and 1200 grits SiC papers. Substrates were cleaned and degreased ultrasonically with acetone for 20 minutes, followed by immersion in 0.1M HCl aqueous solution for 3

minutes. Finally, they were rinsed with deionized water, acetone and ethanol then blow dried using flowing nitrogen gas prior to the spin-coating process.

2.2. Sol preparation and film deposition

The silica based sol was synthesized according to M. Gugliemi et.al by mixing tetraethylorthosilicate ($Si(OC_2H_5)_4$, Sigma-Aldrich), ethanol (C_2H_5OH, Fischer Scientific), hydrochloric acid (HCl, Fischer Scientific), and water in the molar ratio 1:1:5:5.1. The niobia based sol was synthesized by mixing niobium ethoxide ($Nb_2(OC_2H_5)_{10}$, Sigma-Aldrich), ethanol (C_2H_5OH, Fischer Scientific), and glacial acetic acid (CH_3COOH, Fischer Scientific) in the molar ratio1:1:0.5. The resultant niobia and silica sols were magnetically stirred for 15 minutes and 24 hours respectively prior to film deposition. The resultant solutions were spin coated onto the polished stainless steel substrate at 1500 rpm for 35 seconds. The coatings were first dried at 130^{o}C for 12hrs and calcined at 450^{o}C for 4hrs to obtain amorphous coatings. Niobium and Silicon sol precursor concentrations were designed such that a coating of between 100 and 500 nm would be deposited. This was confirmed via both SEM and Laser Profilometry analysis (not shown).

2.3. Preparation of corrosive media

The coated and uncoated substrates were immersed in three different corrosive media; deionized water (pH 7), SBF (pH 7.4) and SGF (pH 1.2) and for 1, 3, 7, 14 and 21 days. The coated substrates immersed in SBF were stored in incubator at 37^{o}C for the specified time periods. High purity deionized water was used for analysis. Simulated body fluid (SBF) was prepared according to the procedure outlined by Kokubo[22]. The reagents were dissolved in 700ml of deionized water using a magnetic stirrer. The solution was maintained at 36.5±0.5^{o}C and the pH of the solution was adjusted to 7.4 by adding Tris (hydroxymethyl) aminomethane and 1 M-HCl. Simulated gastric fluid (SGF) was prepared according to procedure outlined by Asafu-Adjaye et.al. Briefly, 2.0g sodium chloride and 3.2g pepsin (both from Sigma-Aldrich) were dissolved in 7.0ml hydrochloric acid followed by addition of water to make 1000ml solution[23].

*2.4. **Surface Characterization of Coatings***

2.4.1. Scanning Electron Microscopy/ Energy-Dispersive X-ray spectroscopy (FESEM/EDX)

Coatings were observed using FEI Quanta 200F SEM. SEM analyses provided morphological information before and after reaction in different corrosive solutions. The chemical analyses of the sample surfaces were carried out using EDX. In addition, SEM analysis was also used for confirmation of coating thicknesses. FEI Quanta 200F SEM was operated at working distance 7.8mm, accelerating voltage 15kV, and spot size of 3nm. The working distance during EDS was 14mm.

2.4.2. X-ray Photoelectron Spectroscopy (XPS) analysis

The chemical composition as well as local bonding environment of coated and uncoated stainless steel substrates was analyzed with a PHI Quantera Scanning X-ray photoelectron Microprobe (XPS). XPS scans (0-1250 eV) were collected with Al Kα X-rays (monochromatic, beam size=100 µm) at an output power of 25.5 watts, with an electron energy of 1486.6 eV, a step size of ~0.50 eV, a beam dwell time of ~100 ms, and a pass energy of 140 eV. Five different spots, with an approximate analysis area of 1x1mm each were analyzed per sample. The C1s peak of adventitious carbon at 284.60eV was used as a charge reference to determine the binding energies. Significant change in the peak positions of each element, beyond the standard deviation of ±0.15 eV, was not observed. Resultant spectra were analyzed with PHI Multipak V8.0 software as well as the NIST XPS database. A semi-quantitative analysis was deduced by determining the ratio of Cr/Fe from all five spectra for UC-SS.

*2.5. **Electrochemical measurements of the coatings***

2.5.1. Electrochemical Cell Set-up

Electrochemical measurements were conducted in a custom Teflon cell shown in Figure 1. The electrochemical cells were fabricated from solid PTFE rods. A central bore was removed from the main segment of the cell to provide a reservoir for the electrolyte/corrosive media. The working electrode/sample (coated and uncoated stainless steel disk specimens) was laid horizontally and sandwiched between PTFE cylinder and plates. Four screws clamp the entire assembly together. A liquid-tight seal was formed at

the o-ring/wafer interface. The base of the cylinder consisted of a circular hole ~ 6.35 mm in diameter which exposed the selected area of the sample surface to the electrolyte.

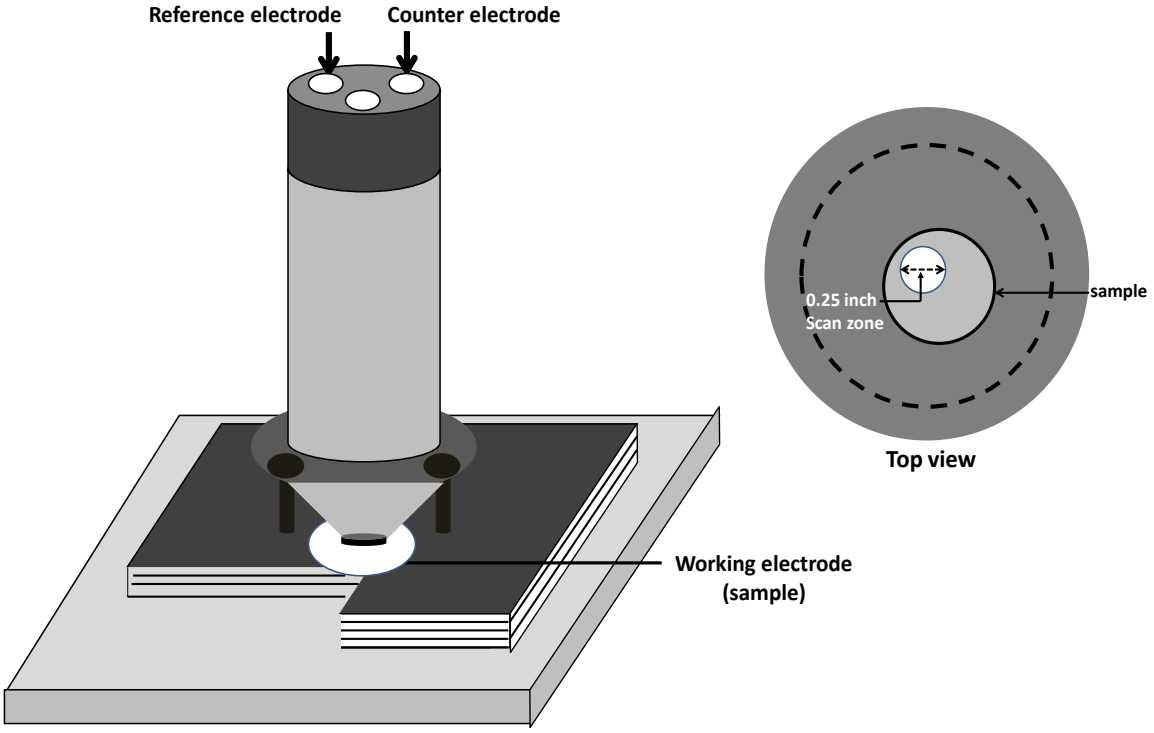

Figure 1. Schematic diagram of custom PTFE electrochemical cell for the disk shaped samples.

During each measurement of this study, the working electrode/sample was mounted leaving a geometrical surface area of 0.32cm^2 exposed to the corrosive media. The bottom piece of PTFE was attached to a metal plate to provide a stable base. A PTFE top piece was fitted over the cell and the reference electrode (RE) and the counter electrode (CE) were placed through holes at the top. They were held in place by rubber rings (not illustrated in figure 1). An Ag/AgCl reference electrode with 1cm^2 surface areas and standard platinum counter electrode wire were inserted into the electrolyte chamber. Measurements were taken from three individual circular sections on the sample surface having same geometrical surface area. The standard deviation represented the error bar in the results. The setup was cleaned with water and acetone after every measurement.

All electrochemical measurements were performed using CH instruments 600 series for open circuit potential (E_{OCP}) linear polarization resistance measurements (Rp).

Before LPR measurement, the Open Circuit potential (E_{OCP}) was recorded for 1 hour. The linear polarization resistances (R_p) were determined at scan rate of $0.1mVs^{-1}$, within the potential range of -20 to 20mV versus the E_{OCP}.

2.5.2. Open circuit potential (OCP)

It is a simple technique which involves immersion of specimen in electrolyte and measurement is recorded for specified time till a stable potential value is obtained. The potential values (E_{OCP}) are recorded with respect to a reference electrode. There is no external current involved during this experiment.

2.5.3. *Measurement of Linear Polarization resistance (LPR)*

The polarization resistance of a material is defined as the slope of potential-current density at corrosion potential (E_{corr}). The polarization resistance R_p that can be related to the corrosion current by Stern-Geary equation:

$$Rp = \frac{B}{i_{corr}} = \frac{(\delta \Delta E)}{(\delta i)}_{i=0, dE/dt \to 0} \qquad \text{Equation (1)}$$

B is Stern-Geary constant, R_p is the polarization resistance and i_{corr} is the corrosion current. The proportionality constant, B, for a particular system can be determined from b_a and b_c, the slopes of the anodic and cathodic Tafel.

$$B = \frac{B_a B_c}{2.3(B_a + B_c)} \qquad \text{Equation (2)}$$

The LPR value is designated as *Rp* and is related to corrosion current i_{corr} by,

$$i_{corr} = \frac{B_a B_c}{2.3 R_p (B_a + B_c)} \qquad \text{Equation (3)}$$

The default values for B_a *and* B_c in the previous equation can be considered as 120mV/decade. The corrosion rate(CR in mpy) is given by,

$$CR = \frac{0.13 i_{corr} (E.W)}{Ad} \qquad \text{Equation (4)}$$

E.W= equivalent weight of the corroding species, g

d= density of corroding species, g/cm^3

A = area of specimen, cm^2

Considering the test is performed on samples with equal surface area the highest Rp value (lowest corrosion rate) corresponds to higher corrosion resistance.

3. Results

3.1. Characterization Pre-immersion in Test Media

3.1.1. Uncoated stainless steel

The SEM micrograph and corresponding XPS spectrum of pristine UC-SS are shown in Figure 2(a) & (d) respectively. The asperity and grid lines on the SEM images resulted from mechanical polishing. At higher magnification (inset image), the surface appeared granular with small round particles~20nm sporadically distributed over the surface. The XPS spectrum (Table I) in the binding energy range from 1250 eV to 0 eV revealed the presence of Cr, Fe, Mo and Ni in addition to C and O. The first four elements from now onwards would be referred as the "substrate elements". Each of the five spots measured per sample showed identical spectra.

3.1.2. Niobium oxide

The SEM micrograph and corresponding XPS spectrum of unreacted Nb-SS coating are shown in Figure 2(b) & (e) respectively. The SEM images showed the presence of crack-free and homogeneous films with no impurities at the surface. At higher magnification (inset image), the microstructure of the coated surface showed tiny circular pores approximately 100-200nm distributed across the surface. The XPS analysis identified peaks for O, Nb, and C only. Each of the five spots measured per sample showed identical spectra.

3.1.3. Silicon oxide

The SEM micrograph and corresponding XPS spectrum of unreacted Si-SS are shown in Figure 2(c) & (f) respectively. The SEM image did not show any observable specific morphological features. The XPS analysis identified peaks for O, Si, and C only. Each of the five spots measured per sample showed identical spectra.

Table I. Elemental Composition of UC-SS, Nb-SS and Si-SS after Immersion in SBF, SGF and Water for 1, 7 and 14 Days

Media	**XPS elemental identification**				
	0 day	**Sample**	**1 day**	**7 days**	**14 days**
SBF	Substrate *	**UC-SS**	Fe, Mo SBF elements*	Fe, Cr, Mo, Mn SBF elements	Fe, Cr, Mo, Mn SBF elements
	Nb	**Nb-SS**	Fe, Mo SBF elements	Fe, Mo SBF elements	Fe, Mo SBF elements
	Si	**Si-SS**	Na, Cl	Fe SBF elements	Fe SBF elements
SGF	Substrate *	**UC-SS**	Fe, Cr, Mo	Fe, Cr, Mo	Fe, Cr, Mo
	Nb	**Nb-SS**	Fe, Cr, Mo	Fe, Cr, Mo	Cr
	Si	**Si-SS**	Fe	Fe	Fe, Cr, Mo
Water	Substrate *	**UC-SS**	Fe, Cr, Mo, Ni	Fe, Cr, Mo, Ni	Fe, Cr, Mo, Ni
	Nb	**Nb-SS**	Fe, Mo	Fe, Mo	Fe, Mo
	Si	**Si-SS**	-	-	-

Substrate: Fe, Cr, Mo, Ni

***SBF elements: Na, Ca, Mg, Cl, P**

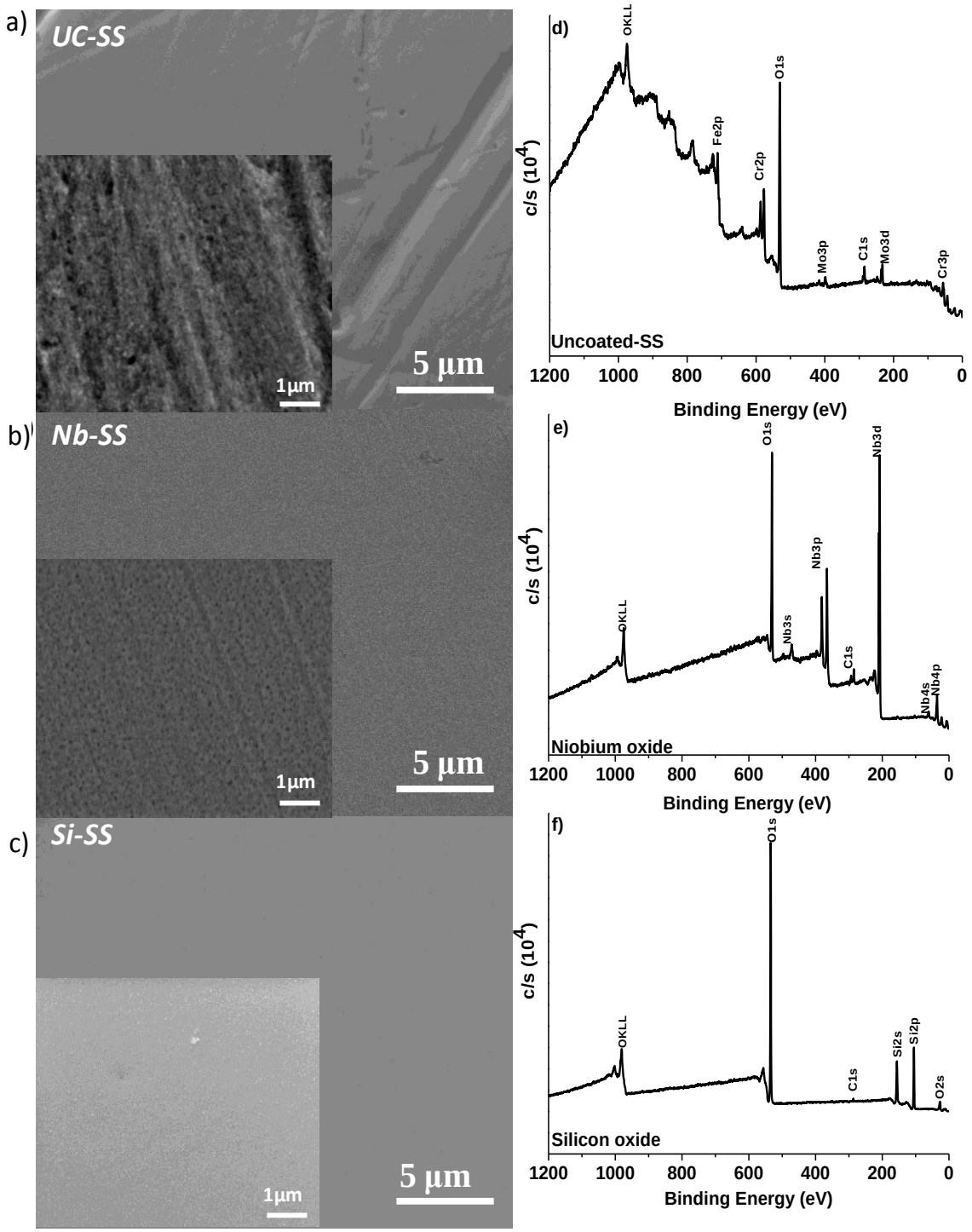

Figure 2. FESEM images (5kx) and corresponding XPS survey scans of (a) UC-SS (b) Nb-SS and (c) Si-SS (inset SEM images are at 20kx).

3.2. Characterization Post-immersion in Test media

FESEM and XPS analyses were performed on UC-SS, Nb-SS and Si-SS after immersion in SBF, SGF and water for 1, 3, 7, 14 and 21 days to investigate the changes in morphology and chemical environment at the sample surfaces as a function of reaction time.

3.2.1. Changes in morphology and surface elemental composition

3.2.1.1. Post immersion in water

Figure 3(a) & (d) showed the surface morphology and corresponding XPS spectrum of UC-SS after immersion in water for 7 days. Polishing scratches ~ 0.5 μm in width was visible on the sample surface for all time periods. At higher magnification, the sample surface appears uneven and granulated after 1-21 day. The XPS survey scans of UC-SS reacted in water were identical to unreacted UC-SS for 1, 7 and 14 days (Table I). XPS spectra peak belonging to all the "substrate elements". Identical XPS spectra were obtained from all five spots measured per sample after 1, 7 and 14 days of water immersion. The Cr/Fe ratio obtained for 1-21 days indicated the formation of Cr rich surface layer (Table II).

Figure 3(b) & (e) show the surface morphology and corresponding XPS spectrum of Nb-SS after immersion in water after 7 days. The coating surfaces after immersion in water for 1 to 21 days did not undergo significant change in morphology. The coated surface did not undergo flaking or peeling off at the surface. The XPS survey scans of Nb-SS reacted in water identified peaks belonging to Fe & Mo in addition to Nb. Identical spectra were obtained from all the five spots measured per sample after 1, 7 and 14 days of water immersion.

Figure 3(c) & (f) show the surface morphology and corresponding XPS spectrum of Si-SS after immersion in water after 7 days. The micrograph obtained after 1-21 days of immersion did not show any significant change in morphology. The XPS survey scans for surface morphology after reaction in water was identical for 1, 7, and 14 days and no peaks for "substrate elements" were observed for any time frame.

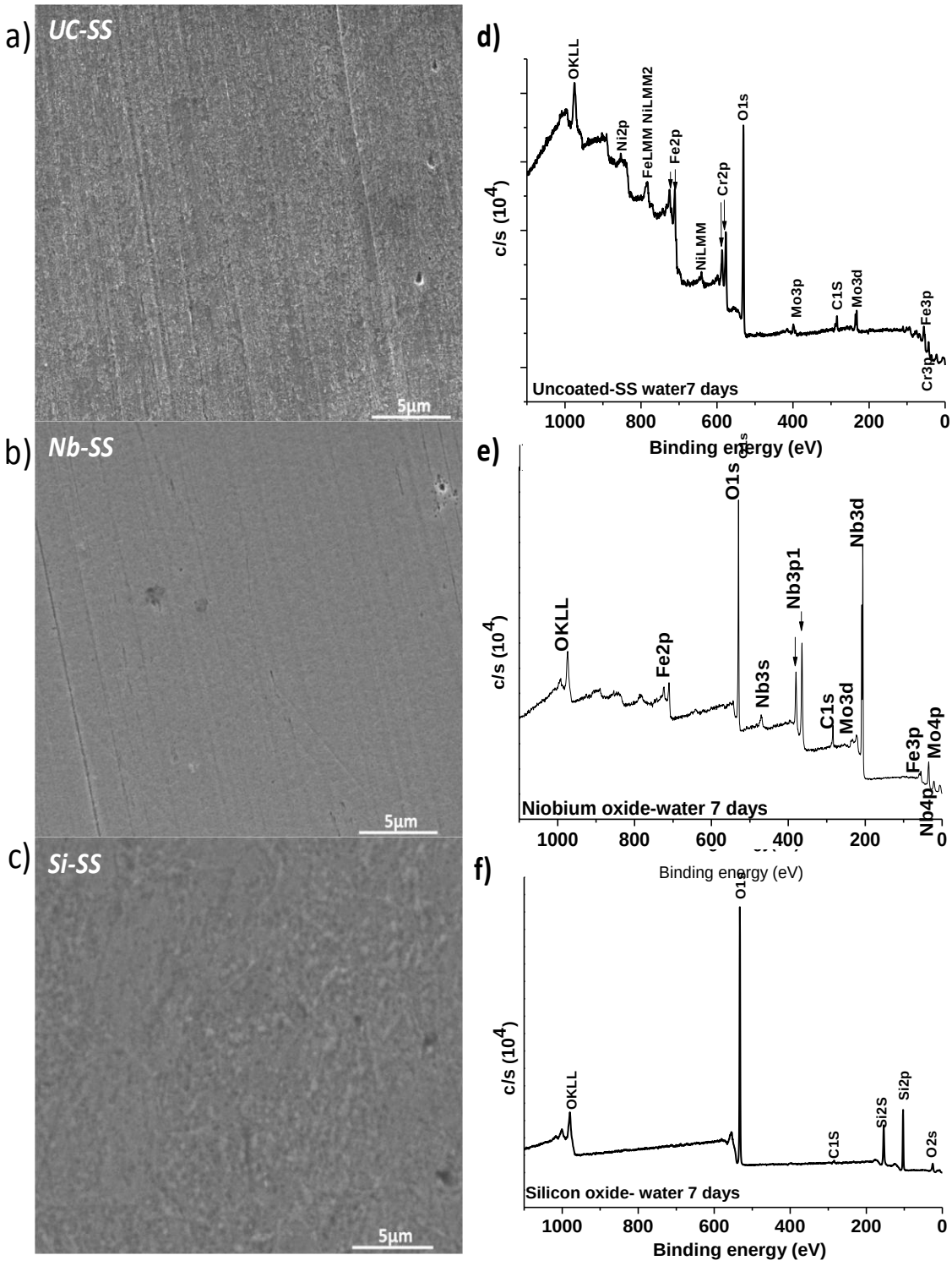

Figure 3. FESEM images of (a) UC-SS (b) Nb-SS (c) Si-SS after 7 days immersion in water and their corresponding XPS survey scans**.**

Table II. Ratio of Cr/Fe on Surface of UC-SS in Different Environments for 1-21 Days

	Ratio of [Cr/Fe] from XPS spectra					
	Days					
Specimen Environment	0	1	3	7	14	21
UC-SS unreacted	0.8	-	-	-	-	-
water		1.0	1.2	1.8	2.2	2.7
SGF		0.3	0.4	0.2	0.9	1.3
SBF		No Cr	0.3	0.3	0.4	0.5

3.2.1.2. Post immersion in SBF

Figure 4(a) & (d) show the surface morphology and corresponding XPS spectrum of UC-SS after incubation in SBF for 7 days. The uncoated surface appeared completely covered with granular particles of sizes ~50-60 nm which was represented by the inset SEM image taken at higher magnification. These granular particles were present at the substrate surface for 1, 3,7,14 and 21 days. Figure 5a shows the surface of UC-SS after 14 days.

The peaks obtained in XPS survey scans of UC-SS after 1day immersion in SBF were identified as Fe, Mo (substrate elements), Ca, P, and some other elements (Na, Mg, Cl, K) deposited from SBF. For convenience, the other elements will be collectively referred as "SBF elements" (Table 2). After 7 and 14 days peaks for Cr & Mn were also observed along with elements observed after 1 day. It was also observed that the peak for P was small for all immersion time periods. Further, the XPS scans obtained from five spots measured per sample were identical for 1, 7 and 14 days. The Cr/Fe ratio for 3-21 days indicated the formation of surface layer with stable composition.

Figure 4(b) & (e) show the surface morphology and corresponding XPS spectrum of Nb-SS after incubation in SBF after 7 days. The microstructure of the coatings after incubation for 1 day showed the presence of small granulated particles ~10-20 nm deposited across the entire surface of coating. After 3, 7, 14 and 21 days deposition of clustered round particles ~ 0.2 μm were observed at the coating surface. The surface also

appeared to develop ~100nm long microcracks at some loactions after 7 days. After 14 days, a mesh like cross linked microstructure was observed at the Nb-SS surface (Figure 5b).

The peaks observed in XPS survey scans for Nb-SS after 1 -21 days of immersion in SBF were identified as Fe, Mo (from substrate), Ca, P and other "SBF elements". Identical spectra were obtained from all the five spots measured per sample after 1 & 7 days SBF immersion. After 14 days, one of the five spots selected for XPS scans did not reveal any peaks for Nb instead the elements identified were Fe, Ca, P and other "SBF elements" only.

Figure 4(c) & (f) showed the surface morphology and corresponding XPS spectrum of Si-SS after incubation in SBF after 7 days. After 1 day, the coating surface was crackfree with small particles ~50-80 nm randomly present at the surface. After 7-14 days, long cracks ~20 μm and width of < 1 μm stretched across the surface layer. These cracks were projected outwards revealing the surface layer below it. After 3days, clustered round particles ~70 nm were observed for the first time at different locations at the surface. They were determined to be composed of Ca and P by EDS analysis. These clustered depositions were observed after 3 days and by 14 days, the surface was extensively covered with these deposits (Figure 5c).

The XPS survey scans for Si-SS after 1 day reaction in SBF show peaks for Na, Cl and Ca from SBF apart from Si, C and O. There were no peaks obtained from the "substrate elements". After 7 and 14 days, peak for Fe was observed along with those for "SBF elements". Further, after 14 days the Si peak intensity was significantly reduced and Ca and P peak intensities increased from all five different spots considered for XPS scans. The elements identified were mainly Ca and P along with other "SBF elements". Each spot measured per sample for different immersion periods showed identical spectra.

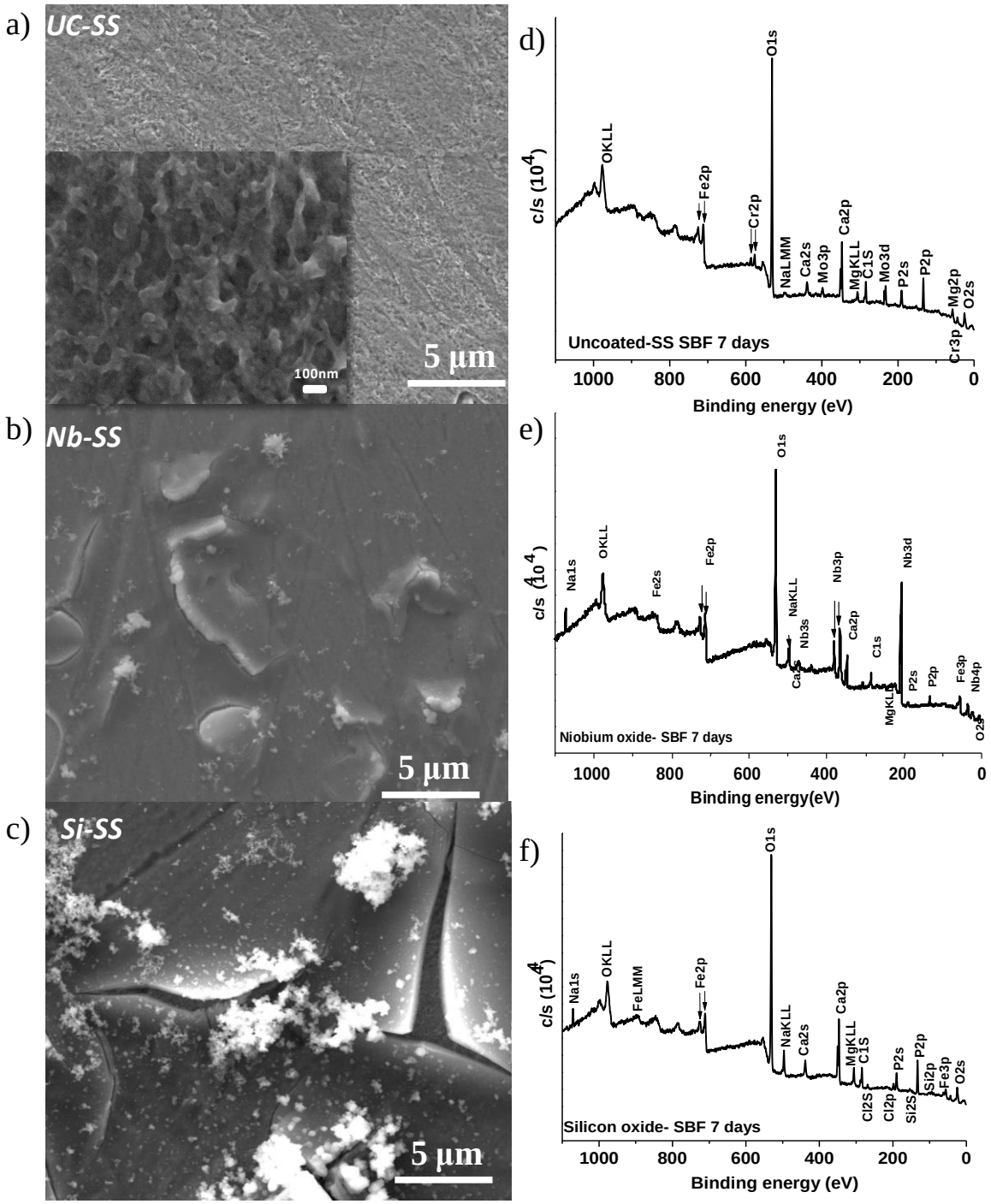

Figure 4. FESEM images of (a) UC-SS (b) Nb-SS (c) Si-SS after 7 days immersion in SBF and their corresponding XPS survey scans.

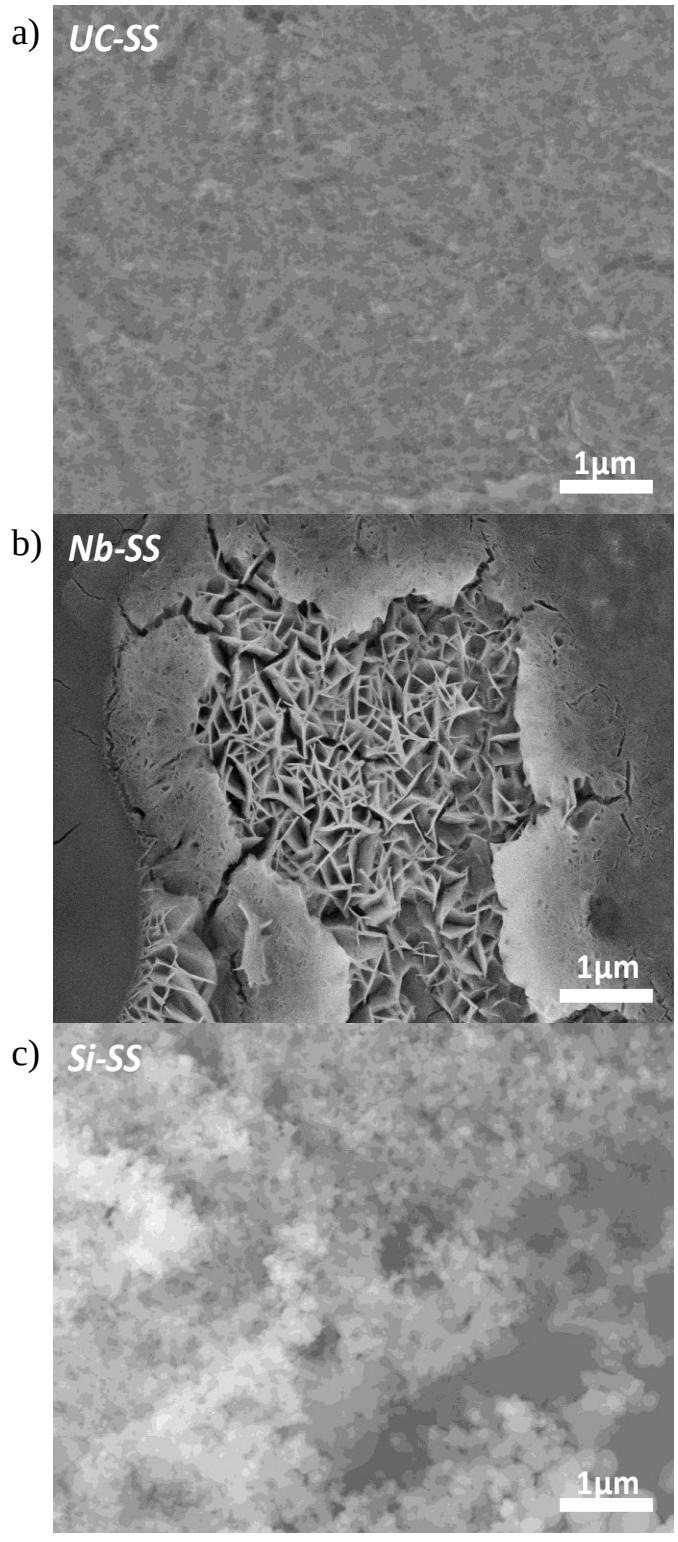

Figure 5. FESEM images of UC-SS, Nb-SS and Si-SS after 14 days immersion in SBF.

3.2.1.3. Post immersion in SGF

Figure 6 (a) & (d) show the surface morphology and corresponding XPS spectrum for UC-SS after 7 days immersion in SGF. The SEM micrograph after 1 day of immersion showed the presence of circular pits <0.2 μm at the surface. The polishing scratches are also visible on the substrates. After 7 days, the surface appeared intensely pitted. The micrographs obtained after 14 -21 days seemed to have less number of circular pits at the surface.

The XPS survey scans for UC-SS reacted in SGF for 1, 7 and 14 days, showed peaks belonging to Na, P and Cl in addition to those belonging to the substrate (Table 3). Identical spectra were obtained from all the five spots measured per sample after 1, 7 and 14 days of SGF immersion. The ratio of Cr/Fe obtained from XPS scans decreased after 1 day and further after 7 days. After 14-21 days, the ratio increased due to passivation of films.

Figure 6(b) & (e) show the surface morphology and corresponding XPS spectrum of Nb-SS after 7 days immersion in SGF. The SEM micrograph at the coating surface show abundant circular pits ~0.3-0.5 μm after 1 day. After 7-14days, appearance of pits and cavities reduced and additionally after 14 days light colored round particles ~0.3μm were observed which by EDS analysis were determined to be composed of Fe, Cr, Mo. Ni and Nb. After 21 days, the light colored particles were no longer visible.

The XPS survey scans for Nb-SS reacted in SGF after 1- 14 day identified peaks for Fe, Cr and Mo from substrate. After 14 days, only Cr peaks were detected from the substrate elements long with peaks for Na and P. After 21 days, peaks for Fe, Cr and Mo from substrate were visible again.

Figure 6(c) & (f) show the surface morphology and corresponding XPS spectrum of Si-SS after 7 days immersion in SGF. After 1 day, the coatings peeled off at some areas on surface in addition to pitting. After 3 days, the surface did not show any peeling but pits and cavities were still visible. After 7 days, the coatings surface again appeared extensively peeled with more pitting at the newly exposed layer. After 14 days, pits and cavities <2.5 μm were visible at the surface along with deposition of ~0.5 μm light colored particles. The pits and cavities after 21 day were smaller <1 μm and coatings appeared smooth with no peeling or delamination.

The XPS survey scans for Si-SS after 1 day reaction in SGF identified peaks for Fe from substrate After 3 days, peaks for both Fe & Cr were visible but only Fe peak was prominent after 7 days. After 14-21 days, peak for Fe, Cr & Mo along with those belonging to coatings was observed. Each of the five spots measured per sample for different immersion periods show identical spectra.

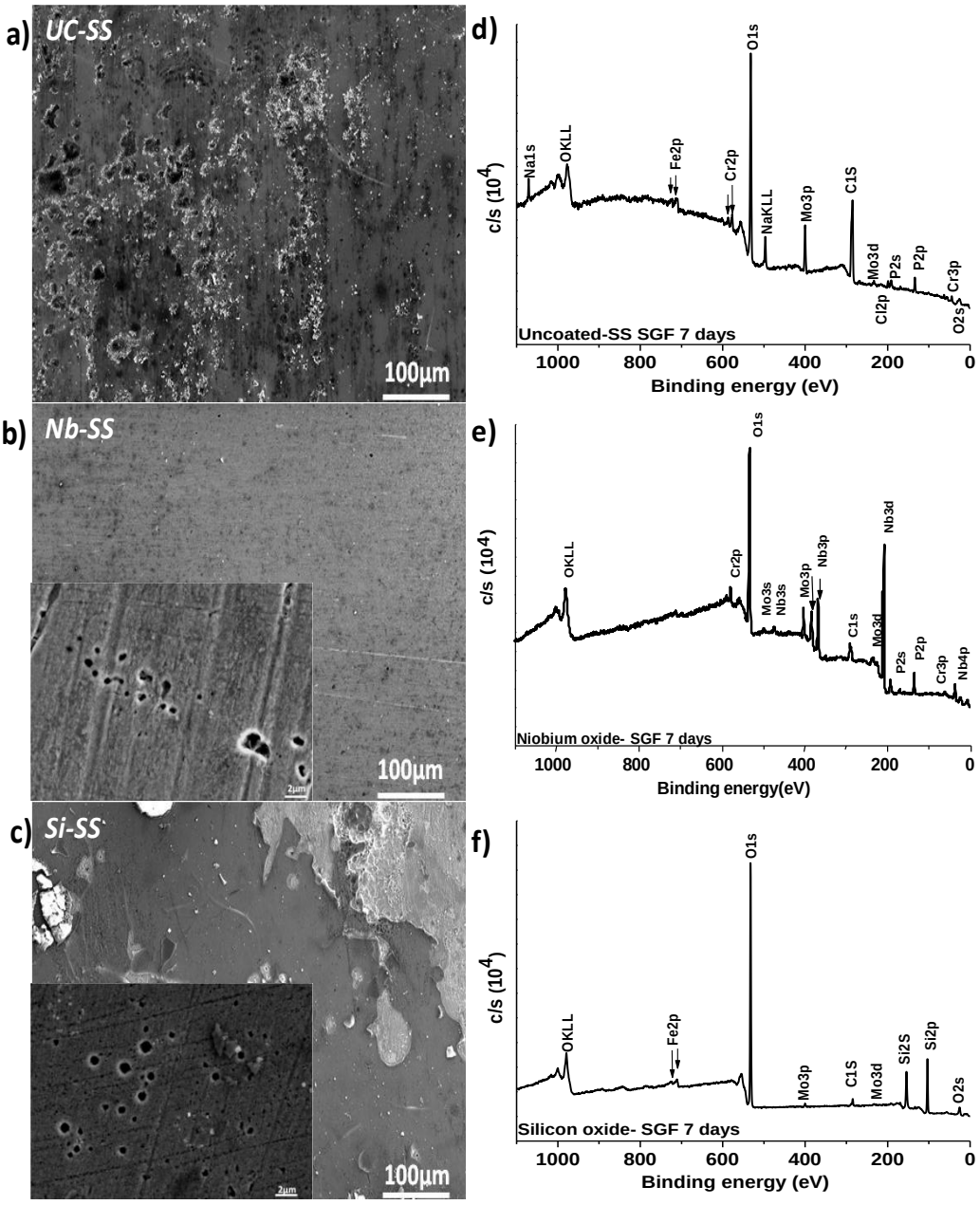

Figure 6. FESEM images of (a) UC-SS (b) Nb-SS (c) Si-SS after 7 days immersion in SGF and their corresponding XPS survey scans.

3.3. Electrochemical analysis

The Open circuit potential (OCP) values and linear polarization resistance values (R_p) were obtained for all coated and uncoated samples which had been previously immersed for 1, 3,7,14 and 21 days in different corrosive media; SBF, SGF and water. Instantaneous corrosion rates after individual time periods were calculated from the R_p value. Three different spots on the same sample were chosen to perform the electrochemical analysis.

The OCP v/s time was conducted prior to measurement of Rp value. The initial and final values of potential were -1V to 1 V respectively. The experiment was conducted for an hour until stable potential values were obtained. The final potential value obtained at the end of the experiment was recorded as E_{OCP}.

For measurement of LPR values, the previously recorded E_{OCP} value was varied within ± 20mV. The potential values were shifted for the next set of ± 20mV until the measurement yield a corrosion potential value corresponding to zero current.

Table III shows the E_{OCP} and Ecorr values obtained after measurements in water, SBF and SGF. On comparing the E_{OCP} and Ecorr values, the Ecorr appeared shifted with respect to their E_{OCP}, suggesting that the coatings still were not at electrochemical equilibrium, even after the one hour of equilibration in OCP conditions. The difference in E_{OCP} and corrosion potential (E_{corr}) are higher for SBF and SGF systems than in water.

From the Figure 7, it can be observed that the range of polarization resistance values Rp in water extended from 0.42 to 1.25MΩ; in SBF from 0.01 to 2.06MΩ and in SGF from 4.00 to 42.64 kΩ. Corrosion rate (CR) was calculated using the equation (2) and are reported in Table IV. The results and discussion will be explained on the basis of Rp value keeping in mind that higher Rp value corresponds to lower corrosion rate (CR).

Table III. OCP and Ecorr values with respect to Ag/AgCl for UC-SS, Nb-SS and Si-SS after Immersion in SBF, SGF and Water for 1-21 Days

Media	Days	UC-SS		Nb-SS		Si-SS	
		E_{OCP}(V)	Ecorr(V)	E_{OCP}(V)	Ecorr(V)	E_{OCP}(V)	Ecorr(V)
WATER	1	0.06	0.02	0.12	0.11	-0.13	-0.13
	3	0.10	0.07	0.17	0.15	-0.02	-0.04
	7	0.07	0.05	0.21	0.20	-0.12	-0.12
	14	0.04	0.03	0.19	0.18	-0.09	-0.11
	21	0.13	0.12	0.22	0.22	0.01	-0.01
SBF	1	-0.06	-0.64	0.04	0.03	-0.22	-0.35
	3	0.05	-0.45	0.02	-0.37	-0.01	-0.31
	7	-0.04	-0.52	-0.23	-0.38	-0.21	-0.38
	14	0.04	-0.39	0.00	-0.26	-0.09	-0.35
	21	0.17	-0.05	0.08	-0.16	0.09	-0.34
SGF	1	-0.02	-0.35	0.34	-0.44	0.15	-0.13
	3	-0.02	-0.32	0.32	-0.44	0.20	0.15
	7	-0.07	-0.51	0.10	-0.46	0.18	0.01
	14	-0.03	-0.50	0.40	-0.35	0.00	-0.13
	21	-0.02	-0.49	0.35	-0.45	0.36	0.16

Table IV. Corrosion Rate for UC-SS, Nb-SS and Si-SS after Immersion in SBF, SGF and Water for 1-21 Days

Media	**Days**	**UC-SS**		**Nb-SS**		**Si-SS**	
		Rp ($M\Omega.cm^2$)	**CR mpy x 10^{-5}**	**Rp ($M\Omega.cm^2$)**	**CR mpy x 10^{-5}**	**Rp ($M\Omega.cm^2$)**	**CR mpy x 10^{-5}**
WATER	1	**0.43**	5.82	**0.87**	2.85	**1.17**	2.13
	3	**0.57**	4.36	**0.87**	2.85	**1.15**	2.16
	7	**0.68**	3.65	**0.90**	2.75	**1.21**	2.06
	14	**0.70**	3.56	**0.92**	2.71	**1.23**	2.02
	21	**0.72**	3.47	**0.93**	2.68	**1.25**	1.99
SBF	1	**0.01**	243.36	**0.33**	7.64	**0.08**	33.15
	3	**0.01**	378.01	**0.53**	4.73	**0.01**	211.30
	7	**0.01**	384.78	**0.14**	17.31	**0.01**	340.49
	14	**0.15**	16.53	**1.09**	2.28	**0.34**	7.39
	21	**0.24**	10.24	**2.06**	1.21	**0.50**	4.98
SGF	1	**0.00**	663.01	**0.02**	160.00	**0.02**	162.24
	3	**0.01**	227.20	**0.02**	119.46	**0.03**	97.58
	7	**0.01**	386.39	**0.01**	180.07	**0.01**	227.72
	14	**0.01**	288.94	**0.03**	97.79	**0.01**	228.34
	21	**0.02**	149.40	**0.02**	127.07	**0.04**	58.40

In water, the linear polarization resistance (Rp) values were higher for both Nb-SS and Si-SS than UC-SS for all time periods. For UC-SS, the Rp value initially increased until 1-7 days. After 7 days, the Rp value remained constant until 21 days. The highest value of Rp was recorded for 21 days (0.72MΩ cm^2). For Nb-SS, the Rp value remained constant for 1-3 days and then increased slightly until 7 days then remained nearly constant until 21 days. For Si-SS, the Rp values were nearly constant until 1 -3 days and then slightly increased after 7 days. The Rp value remained nearly constant for 7-21 days and highest value recorded was 1.25MΩ cm^2 for 21 days. However, the change in Rp values for Si-SS are not statistically significant as we can see the error bars overlap for almost all time periods. The error bars are based off measurements from three different areas on specimen surface.

In SBF, the linear polarization resistance (Rp) values were higher for both Nb-SS and Si-SS than UC-SS for all time periods. For UC-SS, the Rp value was nearly constant until 7 days after which there was a slight increase after 7-21 days. The lowest value of Rp was recorded for 7 days (0.01MΩ cm^2). For Nb-SS, between 1-7 days the Rp value increased after 3 days and dropped back until 7 days. After 7-21 days, there Rp values increased in a nearly linear fashion until 21 days. The highest value of Rp was recorded for 21 days (2.06MΩ cm^2). For Si-SS, the initial Rp value was highest (0.33 MΩ cm^2) after 1 day then it decreased until 7 days. The lowest value recorded was (0.01MΩ cm^2) after 7 days. After 7-21 days, Rp value increased steadily and finally reached 0.50MΩ cm^2 after 21 days.

In SGF, the linear polarization resistance values (Rp) was lowest for UC-SS after 1 day immersion. Between 1 -3 days, the Rp values increased slightly but decreased again until7 days. Finally after 7-21 days, Rp values increased steadily and reached the highest value of 25.48kΩ. For Nb-SS, Rp values were initially low and nearly same as Si-SS after 1 day. Although there was a slight increase in resistance after 3 days, Rp value further decreased from 3-7 days. The highest recorded Rp value was 38.41 kΩ after which it decreased again. For Si-SS, Rp values decreased gradually until 7 days. Then after 7-21days there was a steady increase in Rp value with highest recorded value as 42.64 kΩ after 21 days.

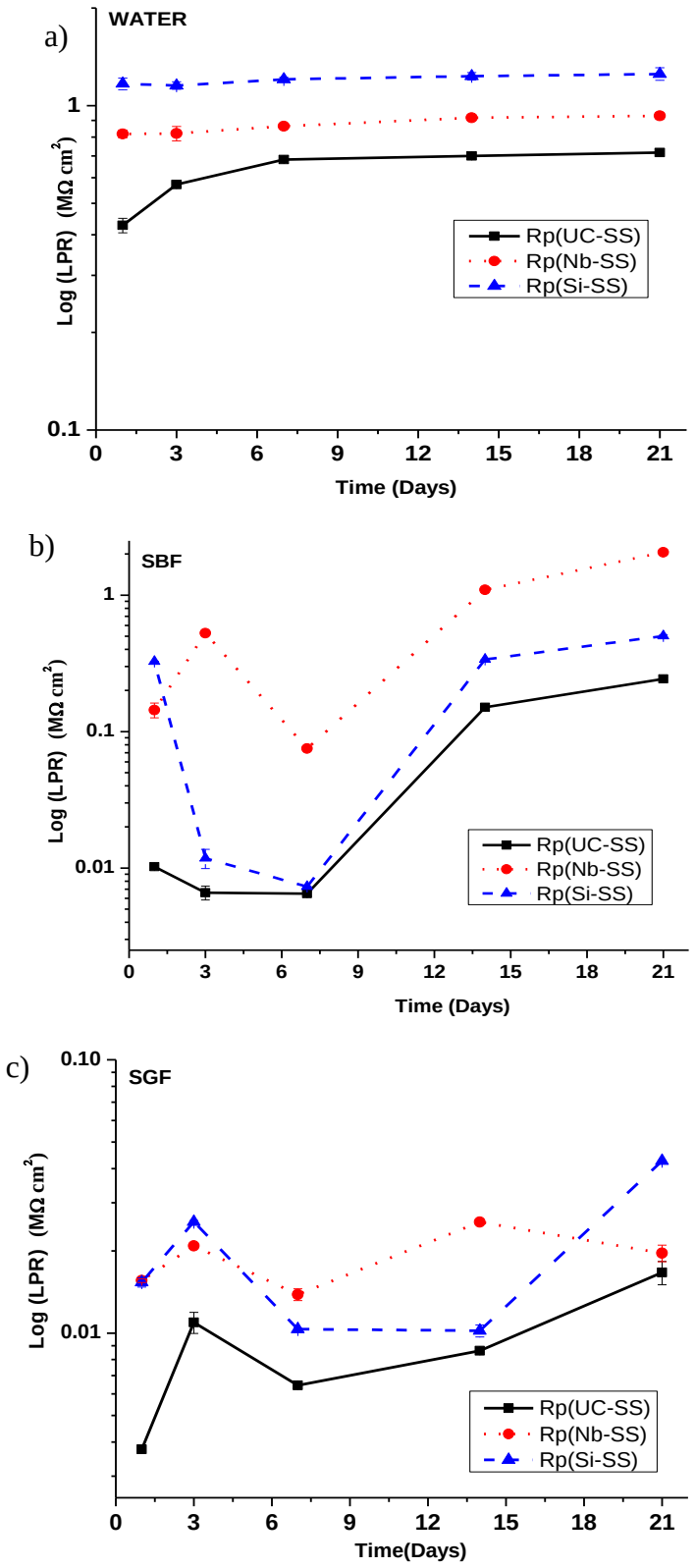

Figure 7. Linear polarization plots for UC-SS, Nb-SS and Si-SS in a) water, b) SBF and c) SGF for 1-21 days.

3.4. Validation of LPR data

In principle, LPR measurements are simple and require a counter electrode to be placed in an electrolyte along with reference and working electrodes. However, LPR measurement is accurate only when the problem of solution resistance (*Rs*) is insignificant. When solution resistance is significant relative to polarization resistance the LPR measurements can be affected. One of the ways to overcome this is by using a three electrode cell set up with extremely high input impedance. For CH instruments, used for present work input impedance of reference electrode is ~ $10^{12}\Omega$ consequently the solution resistance has negligible effect on the values generated.

To verify the accuracy and reproducibility of LPR values, measurement was carried out by placing an uncoated specimen in water. Data was recorded by connecting and disconnecting the Ag/AgCl (reference electrode) and Pt wire (counter electrodes) for 10 different LPR values after every 2 minutes. The standard deviation in Rp values measured was ± 0.0053 for 10 different measurements.

4. Discussion

4.1. Preparation of substrate and coatings

The substrate preparation procedure (polishing of substrate followed by immersion of UC-SS in HCl) imparted surface roughness which enabled better adhesion of coatings onto the substrate. The XPS spectrum for pristine UC-SS showed peak for Cr and Fe with high Cr/Fe ratio0.8 (Table II). The immersion of substrates in acid led to formation of Cr rich layer at the surface.

Both Nb-SS and Si-SS were crack-free and homogeneous prior to immersion as observed in SEM and the absence of substrate peaks in their respective XPS spectrum further validated the point. The Si-SS and Nb-SS were amorphous. However, Nb-SS did show evidence of slight surface porosity. The diameters of these pores are approximately 100-200nm. The pores consisted of 20% of the surface which was calculated using Image J.

4.2. Reaction of samples in water

The presence of a passivation layer on UC-SS in D.I water was indicated by presence of Cr in XPS scans. The increase in Cr/Fe ratio indicated the formation of Cr

rich layer which can be correlated to increase in Rp value over the period of 1-21 days. This indicated that the Cr rich layer is intact and offers some protection against corrosion.

The XPS spectra for Nb-SS show peaks for Fe & Mo for 1-21 days. The SEM micrograph of Nb-SS did show evidence of slight surface porosity and due to this water could have interacted with substrate through the pores which resulted in the substrate peaks (Fe and Mo) being detected in XPS. The SEM analysis did not show extensive degradation of sample which could be due to deionized water being mild medium for corrosion. Molybdenum is often added to stainless steel to improve corrosion resistance. It has been reported that hexavalent molybdenum reacts with active sites from which Fe is removed[24]. Subsequent activity at these sites is therefore reduced, leading to the formation of a more uniform chromium-rich layer. In this way, molybdenum complexes stabilize active sites and prevent the formation of gaps in the passive layer. In this case, there is a possibility that the Mo complex is formed in those nano pores where water may cause dissolution of Fe and therefore Rp value is high.

The XPS spectra for Si-SS did not show any "substrate elements" for 1-21 days. The SEM micrograph also did not show any cracking or peeling of coatings. Further, the Si peak in XPS spectra did not show any decrease in intensity which signified no leaching of silica from coatings. The high Rp value indicated that the coating was intact and durable over the immersed period.

4.3. Reaction of samples in SBF

For UC-SS, the absence of Cr from XPS spectra after 1 day showed that the sample surface did not have any Cr rich layer. However, the Rp value for 1-7 days did not drastically drop which could be due to the presence of Mo. As explained earlier, Mo can form complexes with active sites restricting the dissolution of Fe and consequently improving corrosion resistance. After 7 days, the stainless steel surface contained Cr which indicated presence of passivation layer composed of chromium oxide. This may have resulted in the corresponding increase in Rp value. In UC-SS, even though the XPS spectra identified peaks for both Ca and P the corresponding SEM micrographs do not show any microstructural evidence of Ca and P layer. Further, the XPS peaks corresponding to P on UC-SS was extremely low. So it is difficult to determine whether

the granular particles observed in SEM for UC-SS offered any resistance to corrosion of steel.

For Nb-SS, the nano porous coatings provide a pathway for easy interaction of physiological solution to the substrate in SBF. This may have resulted in the presence of Fe & Mo peaks in XPS after 1 day. Further, the presence of Ca and P peaks after 1 day asserted the biocompatibility of Nb-SS surface. The increase in Rp value after 3 days may be attributed to presence of CaP layer which restricted the interaction of Fe with SBF. After 7 days, small microcracks are visible at the coatings surface which may have resulted in rapid interaction of SBF with fresh underneath layer of uncoated substrate. Hence, even though the CaP layer is still prevalent between 3-7 days the Rp value dropped after 7 days due to dissolution of Fe from microcracks on freshly exposed substrate. The LPR value increased steadily after 14-21 days. This is marked by appearance of mesh-like cross linked structure. This microstructure may belong to CaP layer deposited due to bioactivity of Nb-SS or lepidocrocite (γFe-OOH) which is a corrosion product on stainless steel. Due to high interaction volume, EDS analysis was unsuccessful in indicating the exact identity of the microstructure. However, literature have suggested that both CaP layer as well as γFe-OOH exhibit protective ability corresponding to high Rp value[18,25].

For Si-SS, the SEM and XPS spectra after 1 day were indicative of compact coating which prevented interaction of SBF with the substrate layer underneath. This is supported by highest Rp value which acted as a strong barrier preventing Fe ions dissolution into the physiological fluid. Between 1-3 days, the cracking and peeling of coated surface exposed the underneath which corroded at a different rate due to lower initial polarization resistance of UC-SS. This resulted in drop of Rp value. After 3 days, along with cracking of coatings deposition of light colored particles observed in SEM images which were confirmed to be composed of Ca and P by EDS analysis. After 7 days, severe cracking and peeling of coatings along with CaP layer was prominent. The cracks on silica coatings can be correlated to the presence of Fe in XPS. The XPS spectrum for 7 days does not show the presence of Cr or Mo which indicated that exposed substrate surface was still active. Further, reduction in the peak intensity belonging to Si in respective XPS spectra was also observed which indicated leaching of

silica from the coatings along with cracking. After 14-21 days, the coated surface is covered with CaP layer which has been reported to block the interaction of SBF with the surface improving the corrosion resistance [18].

4.4. Reaction in SGF

The breakdown of Cr rich layer of unreacted UC-SS after 1 day immersion in SGF is evident from the decrease in Cr/Fe ratio in Table II. The breakdown of film may be facilitated by the formation of small pits of the surface presumably due to the presence of Cl^- ions. Between 1-3 days, Cr/Fe ratio increased slightly and so does the Rp value. It shows that presence of a barrier layer on UC-SS can restrict dissolution of Fe. Between 3-7 days, the Rp value decreased and the corresponding SEM after 7 day appeared pitted in abundance. After 7-14 days, pits and crevices on SEM micrograph reduced. This could be due to deposition of corrosion product inside the pits which also facilitated formation of Cr rich layer at the UC-SS surface as shown by Cr/Fe ratio in Table III.

The surface of Nb-SS being slightly porous and it allowed direct interaction of SGF to the substrate underneath. This tends to initiate localized corrosion which is known to be detrimental for stainless steel[71]. The presence of Cr, Mo and Fe along with Nb after 1-3 days indicated that the underlying substrate interacting with SGF did not allow easy dissolution of Fe into the solution. Although the damage due to pitting is evident the total area fraction of pitting was estimated to be insignificant (not shown) which is evident from the increase in Rp value after 3days. Between 7-14 days, the significant increase in Rp value can be correlated to formation of Cr rich layer on the underlying substrates which are in contact with SGF. This is evident from the presence of only Cr peaks in XPS scans after 14 days. After 21 days, the Rp value dropped suggesting the Fe ions dissolution from the substrate.

In Si-SS, the coatings surface appeared peeled for 1 day exposed the underlying region as evident from Fe peak in XPS. The exposed surface consists of pits which facilitated interaction of surface with SGF. It has been reported that the transpassive intermediate layer is formed between the stainless steel and silica[17]. The exposed layer in our coatings could be an intermediate layer as the XPS scans identified the presence of both Si & Fe peaks from five different spots on sample. The absence of other substrate elements further strengthened the argument that the exposed surface after peeling was not

similar to UC-SS. This could be the reason for higher Rp value of Si-SS for 1 day. Between 3-7 days, the surface layer peeled again exposing a fresh surface. This layer will interact with SGF in a different rate which is evident from drop in Rp value. The XPS after 7 days revealed a highly reactive surface containing only Fe from substrate. Due to continuous peeling, Cl^- ions can penetrate more easily through the thinner layer containing pits. This results in substrate ions Fe, Mo and Cr detected in XPS at the surface after 14 days. Finally, after 21 days, the presence of Mo and Cr restricts the dissolution of Fe causing increase in Rp value.

5. Conclusion

UC-SS and sol- gel prepared amorphous Nb-SS and Si-SS were immersed in deionized water, SGF and SBF. The corrosion resistance was evaluated using SEM, XPS and LPR measurement. In water, the UC-SS developed a passivation layer with Cr/Fe ratio increasing with time of immersed. Both Nb-SS and Si-SS did not undergo extensive degradation in SEM and corresponding LPR values were nearly constant throughout the immersion time period. In SBF, the LPR values did not show much variation for UC-SS except after 7 days small increase in LPR was observed after 7 days which could be attributed to formation of a Cr rich layer. The LPR value for Nb-SS was consistently high due to the presence of calcium and phosphate layer and no major cracking of coatings. Since the surface of Si-SS showed extensive cracking and peeling after 7 days drop in LPR values were observed. In SGF, Si-SS surface was peeled after 1 and 7 days while the inherent porosity in Nb-SS allows the solution to interact with substrate easily. The Cl- ions in SGF caused pitting at the surface of coated and uncoated stainless steel.

The LPR values in water for UC-SS were significantly higher than other two media. The LPR value in SBF and SGF for UC-SS were nearly same. The LPR values in water for Nb-SS were highest followed by SBF and then SGF. The presence of Ca and P layer restricted Fe dissolution in SBF while presence of Cl- ions caused pitting of surface and inherent porosity allowed easy interaction of SGF with substrate underneath the coating. The LPR values in Si-SS were highest for water but due to cracking and peeling of coatings the Rp values were nearly same for SBF and SGF.

REFERENCES

1. C. García, S. Ceré, and A. Durán, "Bioactive coatings prepared by sol–gel on stainless steel 316L," *J. Non-Cryst. Solids*, **348** [0] 218-24 (2004).

2. A.-M. CANTARAGIU, G. Carac, and C. Gheorghies, "Electrochemical study of AISI 316L Stainless Steel in different nanoparticle suspensions," *J. optoelectro.s adv. mater,* **12** [12] 2391-9 (2010).

3. P. Rojas and S. Rodil, "Corrosion behaviour of amorphous niobium oxide coatings," *Int. J. Electrochem.Sci,* **7** [2] 1443-58 (2012).

4. D.C. Hansen, "Metal corrosion in the human body: the ultimate bio-corrosion scenario," *The Electrochem.Soc. Interf,* **17** [2] 31 (2008).

5. R. Bhola, S.M. Bhola, B. Mishra, and D.L. Olson, "Corrosion in titanium dental implants/prostheses–a review," *Trends in Biomater. and Arti. Organs,* **25** [1] 34-46 (2011).

6. Y.-C. Tang, S. Katsuma, S. Fujimoto, and S. Hiromoto, "Electrochemical study of Type 304 and 316L stainless steels in simulated body fluids and cell cultures," *Acta Biomaterialia,* **2** [6] 709-15 (2006).

7. S. Hosseinalipour, A. Ershad-Langroudi, A.N. Hayati, and A. Nabizade-Haghighi, "Characterization of sol–gel coated 316L stainless steel for biomedical applications," *Prog. Org. Coat.,* **67** [4] 371-4 (2010).

8. J. Gallardo, A. Durán, and J.J. de Damborenea, "Electrochemical and in vitro behaviour of sol–gel coated 316L stainless steel," *Corrosion Science,* **46** [4] 795-806 (2004).

9. K. Feng, Z. Li, X. Cai, and P.K. Chu, "Corrosion behavior and electrical conductivity of niobium implanted 316L stainless steel used as bipolar plates in polymer electrolyte membrane fuel cells," *Surf. Coat.Technolo,* **205** [1] 85-91 (2010).

10. K.-K. Chew, S.H.S. Zein, and A.L. Ahmad, "The corrosion scenario in human body: Stainless steel 316L orthopaedic implants," *Natural Science,* **4** [3] (2012).

11. A.R.H. Bidhendi and M. Pouranvari, "Corrosion study of metallic biomaterials in simulated body fluid," *Metalurgija,* **17** [1] 13-22 (2011).

12. T.L. Metroke, R.L. Parkhill, and E.T. Knobbe, "Passivation of metal alloys using sol–gel-derived materials—a review," *Prog. Org. Coat,* **41** [4] 233-8 (2001).

13. C.-C. Shih, C.-M. Shih, Y.-Y. Su, L.H.J. Su, M.-S. Chang, and S.-J. Lin, "Effect of surface oxide properties on corrosion resistance of 316L stainless steel for biomedical applications," *Corrosion Science,* **46** [2] 427-41 (2004).

14. G. Ramírez, S.E. Rodil, S. Muhl, D. Turcio-Ortega, J.J. Olaya, M. Rivera, E. Camps, and L. Escobar-Alarcón, "Amorphous niobium oxide thin films," *J. Non-Cryst. Solids,* **356** [50–51] 2714-21 (2010).

15. P. Rojas and S. Rodil, "Corrosion Behaviour of Amorphous Niobium Oxide Coatings," *International Journal of Electrochemical Science,* **7** [2] (2012).

16. J. Ballarre, I. Manjubala, W.H. Schreiner, J.C. Orellano, P. Fratzl, and S. Ceré, "Improving the osteointegration and bone–implant interface by incorporation of bioactive particles in sol–gel coatings of stainless steel implants," *Acta Biomaterialia,* **6** [4] 1601-9 (2010).

17. D.C.L. Vasconcelos, J.A.N. Carvalho, M. Mantel, and W.L. Vasconcelos, "Corrosion resistance of stainless steel coated with sol–gel silica," *J. Non-Cryst. Solids,* **273** [1–3] 135-9 (2000).

18. S.A. Pauline and N. Rajendran, "Biomimetic novel nanoporous niobium oxide coating for orthopaedic applications," *Appl. Surf.Sci,* **290** 448-57 (2014).

19. A. Motalebi, M. Nasr-Esfahani, R. Ali, and M. Pourriahi, "Improvement of corrosion performance of 316L stainless steel via PVTMS/henna thin film," *Progress in Natural Science: Materials International,* **22** [5] 392-400 (2012).

20. C. Garcia, S. Cere, and A. Duran, "Bioactive coatings prepared by sol–gel on stainless steel 316L," *J. Non-Cryst. Solids,* **348** 218-24 (2004).

21. M. Sun, K. Xiao, C. Dong, and X. Li, "Electrochemical corrosion behavior of 300M ultra high strength steel in chloride containing environment," *Acta Metall. Sin.(Engl. Lett.),* **23** 301-11 (2010).

22. T. Kokubo and H. Takadama, "How useful is SBF in predicting in vivo bone bioactivity?," *Biomaterials,* **27** [15] 2907-15 (2006).

23. E.B. Asafu-Adjaye, P.J. Faustino, M.A. Tawakkul, L.W. Anderson, X.Y. Lawrence, H. Kwon, and D.A. Volpe, "Validation and application of a stability-indicating HPLC method for the in vitro determination of gastric and intestinal stability of venlafaxine," *J. Pharmaceutical and Biomed.l Anal.,* **43** [5] 1854-9 (2007).

24. S.J. Kerber and J. Tverberg, "Stainless steel: surface analysis," *Advanced materials & processes,* **158** [5] 33-6 (2000).

25. Y. Xie, Y. Wang, and Y. Men, "Influence of Lepidocrocite Film Formed in-situ on Corrosion Behavior of Weathering Steel in the Solution without Cl," *Int. J. Electrochem. Sci*, **7** 10679-84 (2012).

CHAPTER IV: SOL GEL PREPARED NIOBIUM OXIDE COATINGS ON 316L STAINLESS STEEL AS CARRIER OF ERYTHROMYCIN

D. Pradhan[1], *A.W. Wren*[1], *N.P. Mellott*[1,2]*

[1]Inamori School of Engineering, Alfred University, Alfred, NY 14803 USA.

[2]Department of Chemical Engineering and Materials Science, Michigan State University, East Lansing, MI 48842

Keywords: Erythromycin, Niobium oxide, Drug loading

*To whom all correspondence should be addressed.

Nathan P. Mellott
428 S. Shaw Lane
Department of Chemical Engineering and Materials Science
Michigan State University
East Lansing, Mi 48824
mellott3@egr.msu.edu
Ph: 607-760-4944

Abstract

Erythromycin in different concentrations (10, 40 and 80 mg/ml) was incorporated into niobium oxide coatings on stainless steel via solution route and incipient wetness impregnation route. The effects of drug incorporation in the coatings were evaluated via SEM images. The release of erythromycin in PBS was measured using UV-Vis spectroscopy and short term antibacterial properties were analyzed for 3 and 24 hours. Further, the adhesion of *S.aureus* on the drug containing surface were also observed using SEM. A comparative study for release and antibacterial properties of erythromycin containing niobium oxide coatings was made based on two different processing routes, variation in drug concentration and time of immersion.

1. Introduction

Implanted biomaterials particularly used for joint fixation or replacement serves as an ideal platform for bacterial colonization. This colonization often leads to periprosthetic infection (PPI) causing destruction of local tissues, patient disability and morbidity and may even require surgical removal of the implant [1]. Currently, PPI requires removal of contaminated implant coupled with extensive bone debridement and prolonged antimicrobial treatment[1]. Therefore, a combination devices that can work as an implant and release therapeutics in controlled manner at the target sites, and lower infections needs to be developed. According to US FDA's definition "a combination device comprises of two or more regulated components(drug/device) that are physically and chemically combined to produce a single entity"[2,3]. This could possibly decrease systemic toxicity and risk of fostering bacterial resistance [2,4]. It is also hypothesized that local delivery of drugs may yield higher drug concentration in the relevant tissues thereby improving efficacy and possibly reducing the healing time[5]. Recently, antibiotic impregnated sol-gel matrices are under investigation[1,6-10].

The implementation of sol-gel methodology enables a number of advantages over other coating techniques such as increased homogeneity as mixing occurs at atomic level; and the ability to coat complex shapes[11,12]. Drug release behavior can be affected by changing the sol-gel processing parameters[13]. The possibility of encapsulating antibiotics into metal oxide matrices using sol-gel technique offers new possibilities for drug delivery. The release properties can be tailored by modifying the nanostructure of gel network and embedded drug [10]. For efficient drug delivery, the carrier should be nontoxic and exhibit good biocompatibility [13,14]. Currently, the controlled release of from various silica and titania matrices, calcium phosphate and hydroxyapatite coatings have been extensively studied[1,5,10,15-17]. Niobium oxide which has been relatively less studied than silica has been known to offer excellent biocompatibility, good inherent porosity and excellent adhesion to stainless steel.

In the present study, niobium oxide coatings on stainless steel prepared via a modified sol-gel route have been loaded with erythromycin in three different concentrations (10, 40 and 80mg/ml). The antibiotic was incorporated via two possible

routes; a solution and incipient wetness impregnation route. Furthermore, short term antibacterial properties, bacterial viability, and antibiotic elution were investigated.

2. Materials & Methods

2.1. Coating Processing and Deposition

Niobium based sols were prepared by mixing 5.14 g of glacial acetic acid (Fischer Scientific) in 3.95 g of ethanol (Fischer Scientific) in a glass vial. Next, 0.27 gm of niobium ethoxide (Sigma-Aldrich) was added to the mixture. The transparent sol containing glass vial was sealed with parafilm and stirred using a magnetic stirrer for 20 minutes. A second , erythromycin containing sol was prepared in which 10, 40 and 80 mg of erythromycin per 1ml of sol was added under constant stirring and further stirred for 15 minutes to allow the antibiotic to fully dissolve.

Preparation of Erythromycin loaded coatings were then prepared by two different methods; the solution route (SR) and the incipient wetness impregnation route (IWIR). First, medical grade stainless steel (316L) circular discs (~21mm in diameter, Swagelok) were ground with 600 and 1200 grit SiC paper to a uniform finish. The substrates were then sonicated for 15 minutes in acetone and rinsed with DI water to remove any leftover residual particulates from grinding. Next, they were immersed in HCl for 5 minutes and rinsed in sequence with D.I. water, acetone and ethanol. Finally, each substrate was dried using nitrogen.

SR-coatings were prepared through the spin coating of the erythromycin loaded sols at 1500 rpm for 35 seconds, followed by a 60^{o}C heat soak for 20 minutes. A second spin coated layer was then deposited at 1500 rpm for 35 seconds and air dried overnight and stored in a sealed petri dish. The coatings prepared by this route are named as NbSR-10E, NbSR-40E and NbSR-80E.

IWIR sols were prepared via spin coating of the initial niobium sol at 1500 rpm for 35 seconds, followed by a 130^{o}C heat soak for 20 minutes. A second spin coated layer was then deposited at 1500 rpm for 35 seconds followed by a 450 C heat treatment for 4 hours. The resultant niobium oxide coatings were then immersed into a 3ml simulated body fluid (SBF) solution containing 10, 40 and 80 mg/ml of erythromycin and kept in an incubator at 37^{o}C for 96 hours. After 96 hours, the discs were taken out using forceps,

rinsed in water and dried at 37^{o}C for 1 hour in the incubator. The coatings prepared by this route are named as Nb450-10E, Nb450-40E and Nb450-80E.

2.2. Coating Release of Erythromycin

The erythromycin release from the coated samples was determined as a function of soaking time in 4ml of phosphate buffer solution (PBS) for 3 and 24 hours. After each immersion period, the PBS solution extracts were collected from the individual well plates and the coated samples were removed, rinsed with deionized water and dried. The PBS solution collected was measured spectrophotometrically using UV-Vis spectrophotometer Perkin Elmer lamda 950 to evaluate the concentration of erythromycin released[18]. Through the development of a calibration curve, molar absorptivity (ε) of erythromycin was determined as 20.52 L mol^{-1} cm^{-1} and concentration of erythromycin was calculated using the Beer -Lambert law A=εcl.

2.3. Coating Performance vs. S. aureus

The bacterial culture solution was initially prepared by removing a colony of *S.aureus* bacteria from the culture plate with inoculating loop and adding it to 5ml of Tryptic Soy broth (TSA) broth in a 15ml tube. This solution was vigorously mixed and incubated at 37^{o}C for 24 hours. After 24 hours, the bacterial culture solution was removed from the incubator and used for different bacterial tests.

The bactericidal activity of the coated samples was evaluated against *S. aureus* using a modified spread plate technique[19]. The samples were placed under UV light overnight and then washed in ethanol (80%) for few seconds and dried. This was followed by transfer of samples to a sterilized six well plate prior to bacterial testing. Next, a bacterial suspension of *S.aureus* was prepared by mixing 40µl of bacterial culture solution in 960µl of sterile deionized water in a sterilized conical tube and vortexed vigorously. Then, 150µl of diluted solution was pipetted onto each sample surface, sealed to prevent the bacterial suspension from drying, and left in a chamber for 3 hrs. After 3 hours, the suspensions at the sample surfaces were collected using a cotton swabs and spread on a 20ml agar containing petri dishes. The agar petri dishes were incubated at 37^{o}C for 24 hours to allow the formation of bacterial colonies. The formation of bacterial colonies on coated samples and uncoated samples (control) were compared to evaluate their bactericidal activity.

The bacterial viability was determined by placing sterilized samples, and the above mentioned bacterial culture solution, in six well plates. The volume of bacterial culture solution taken depended on the number of samples for analysis. After placing the samples, 3ml of bacterial-broth solution were pipetted into each well. The bacterial culture solution was vigorously mixed prior to pipetting 3ml in each sample well and the set up was incubated at 37^{o}C for 24 hours. After 24 hours, 100µl of solution extracts were pipetted from individual well (n=6) and aliquots were added to a 96 well plates. Finally, the plate reader was used to calculate the bacterial viability by measuring absorbance at 570nm. The uncoated samples were assumed to have 100% bacterial viability. The uncoated substrate and drug loaded coatings were imaged under Scanning electron microscopy (SEM) to observe the surface after immersion in bacterial broth.

3. Results and Discussion

3.1. Coating Processing and Deposition

The choice of the precursor for this study was based on previous investigation where a stable niobium based sol was successfully prepared for deposition of the coating[20]. The Erythromycin was added in small quantities using a spatula to successfully prevent precipitation even at high loading concentrations. The antibiotic fully dissolved in the sol giving a clear and transparent solution for deposition on stainless steel. The SR-coatings were spatially homogeneous with no evident cracks or pores at the surface; although minimal polishing scratches were visible (Figure. 1). The SR-coatings loaded with 10 mg/ml consisted of light colored particles deposited on the polishing scratches as well as other areas of coatings while those loaded with 40 and 80 mg/ml of erythromycin appeared smooth and homogenous. IWIR-coatings, regardless of loading concentration appear spatially homogeneous (Figure 1) with calcium phosphate deposited on the surface confirmed by EDS (not shown).

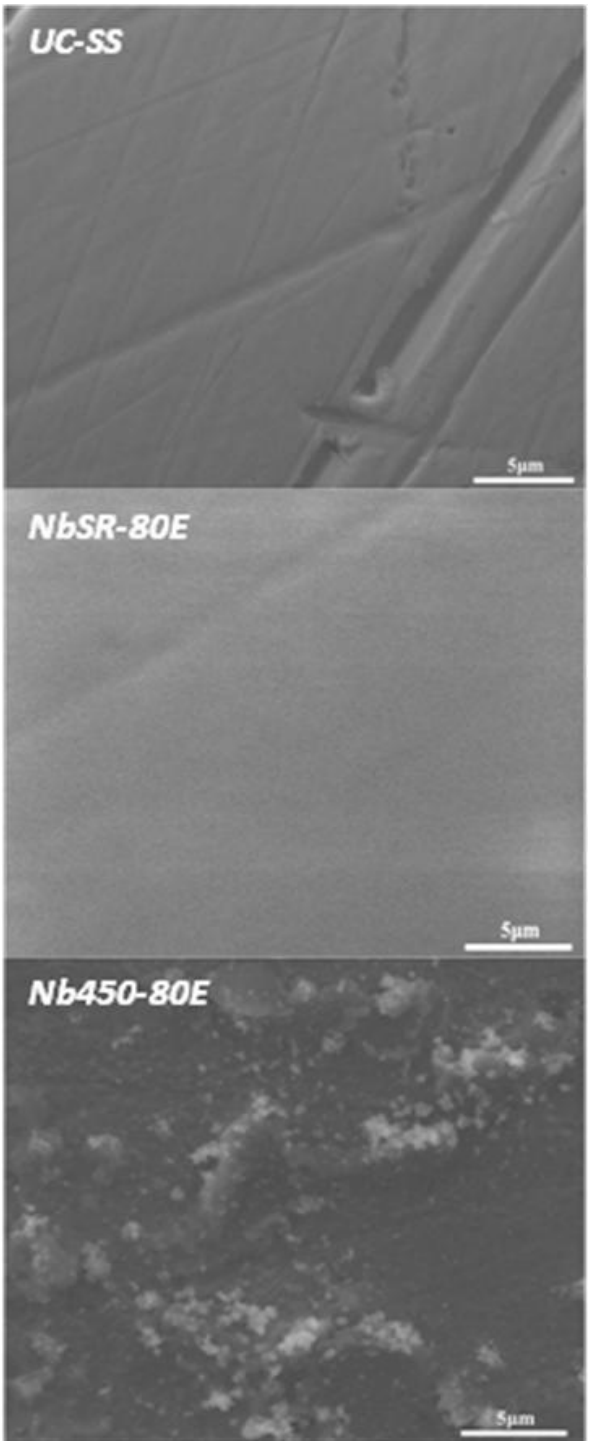

Figure 1. Scanning electron microscope image of the surface of UC-SS, NbSR-80E, and Nb450-80E prior to exposure to bacteria.

3.2. Coating Release of Erythromycin

The concentration of erythromycin released in PBS after 3 and 24 hours as a function of processing method, erythromycin concentration, and time of immersion is shown in Table I. For SR-coatings the concentration of erythromycin released increased with increasing loading concentration. Erythromycin is not detectable in solution after reaction for 24 hours with the IWIR-coatings with 10 mg/ml erythromycin. For IWIR-coatings with 40 and 80 mg/l erythromycin, the concentration released was found to increase with higher loading concentrations after 24 hours. Overall, antibiotic elution from SR-coatings was higher in comparison to that from IWIR-coatings. The release of erythromycin in PBS for both SR and IWIR-coatings increased with time of immersion.

Table I. Concentration of Erythromycin Released from Coatings after 3 and 24 hours Immersion in PBS as Determined using UV-Vis Spectrophotometer

Sample	**Concentration (mg/ml) after 3 hrs**	**Concentration (mg/ml) after 24 hrs**
NbSR-10E	0.22	0.76
NbSR-40E	0.49	5.57
NbSR-80E	2.46	7.78
Nb450-10E	-	-
Nb450-40E	0.30	0.95
Nb450-80E	0.31	1.30

It has been reported that the initial burst of antibiotic released from system should be high enough to counter the initial elevated infection risk immediately post implantation[3]. The initial release (3 hours) of erythromycin from NbSR-80E was higher than the minimum inhibitory concentration (MIC) for *S.aureus* (0.5mg/ml)[21]. According to the literature, the primary mechanism for release of drug from SR coatings is by degradation of films. The rate of degradation increased with higher concentration of drug in coatings[6,7]. This indicated that film dissolution plays a major role in drug release from sol-gel thin films.

According to the literatures, the primary mechanism for release through IWIR coatings is diffusion of the drug from the matrix, and not due to dissolution of carrier. The release rate in this system is expected to be rapid initially followed by gradual and continuous delivery[12]. However, the presence of CaP layer may alter the mechanism of incorporation/release of drug from the system[16]. During incorporation the drug molecule is known to bind with Ca and P ions[22]. Although the role of Ca and P ions during release is not absolutely clear there is a possibility that its presence might restrict drug release from the system. Since the current work is limited to 24 hours it is difficult to provide a detailed observation on the role of CaP layer.

3.3.Coating Performance vs. S.aureus

Figure 2 shows the results of bactericidal activity for UC-SS, NbSR-80E and Nb450-80E after 3 hours of dripping bacterial suspension on the sample surfaces. Both SR and IWIR coatings containing 40 and 80mg/l erythromycin showed enhanced bactericidal activity in comparison to those containing 10mg/l erythromycin. After 3 hours, it was evident that the UC-SS agar plate had abundant colonies of bacteria grown and the release of erythromycin from NbSR-10E and Nb450-10E was insufficient to eradicate all the bacterial colonies (not shown). This experiment could not be performed for longer time periods as the bacterial suspension at the surface of samples dried up rapidly. However, it was evident that the presence of erythromycin containing niobium coatings on stainless steel helped improve the bacterial resistance in comparison to bare UC-SS which showed a lack of any bactericidal activity.

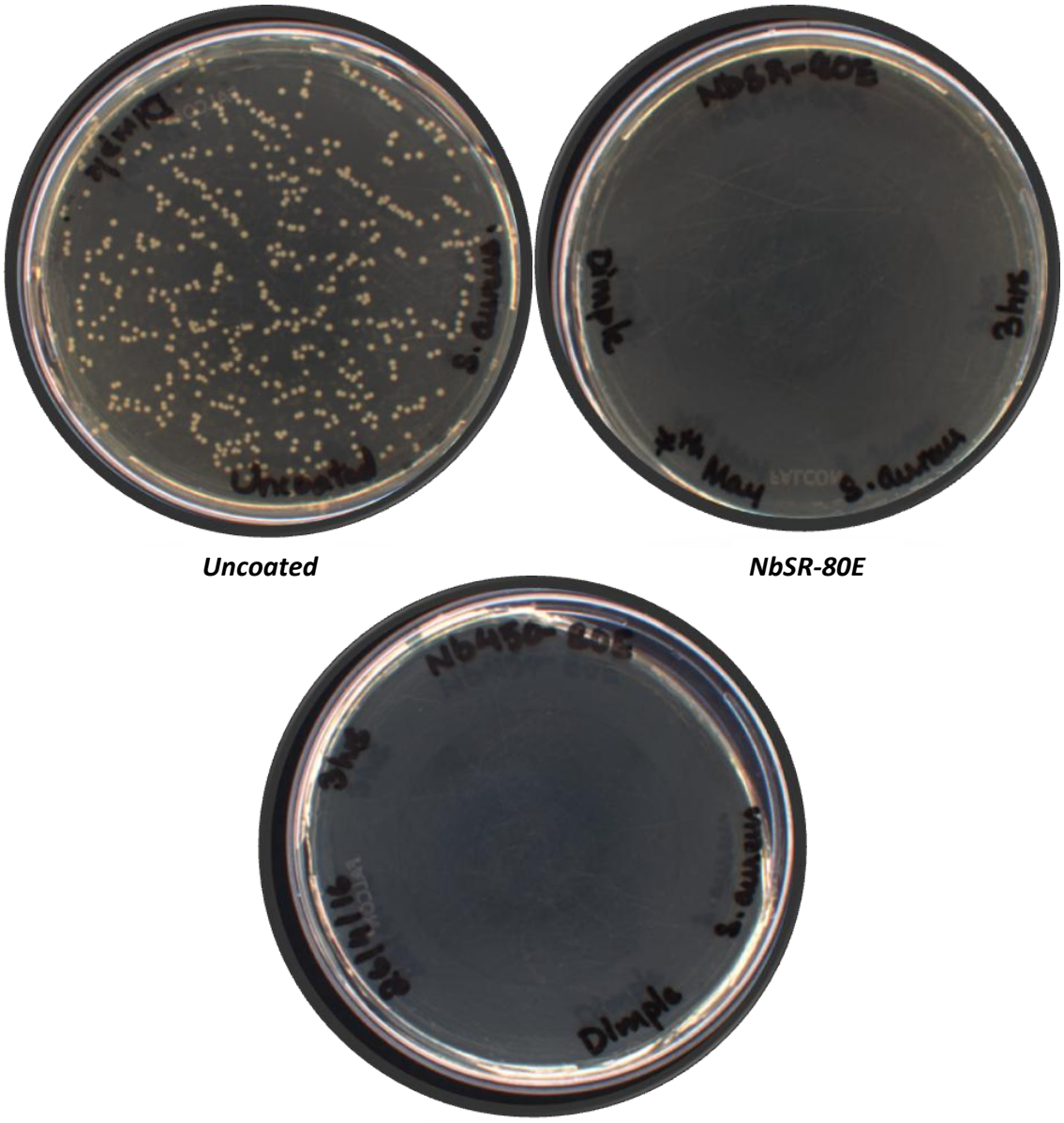

Figure 2. Bacterial colony formation images of UC-SS, NbSR-80E, and Nb450-80E after 3 hours of exposure to bacterial solution.

Figure 3 compared the bacterial viability as a function of processing method, erythromycin concentration, and time of immersion. Bacterial viability for drug loaded samples was compared to the UC-SS which is assumed to have bacterial growth of 100%. For SR coatings, the reduction in bacterial viability was highest for NbSR-80E coatings (~ 63%) and lowest for NbSR-10E (~19.3 %) after 24 hours in comparison to the control

sample (UC-SS). SR coatings containing 40 and 80mg/ml erythromycin showed similar results after 24 hours. For IWRI coatings, the reduction in bacterial viability was highest for Nb450-80E coatings (~44%) after 24 hours and lowest for Nb450-10E (~15%) after 24 hours in comparison to the control sample (UC-SS). IWIR coatings containing 40 and 80mg/ml erythromycin showed similar results after 24 hours. It was observed that SR coatings provided greater bacterial resistance in comparison to IWIR coatings for both 3 and 24 hours.

The results also indicated that bacterial resistance improved with increase in time of immersion except for Nb450-10E where bacterial viability after 3 and 24 hours were nearly same. However, the increase in concentration of erythromycin did not correspond to increase in bacterial resistance after addition of more than 40mg/ml erythromycin in coatings.

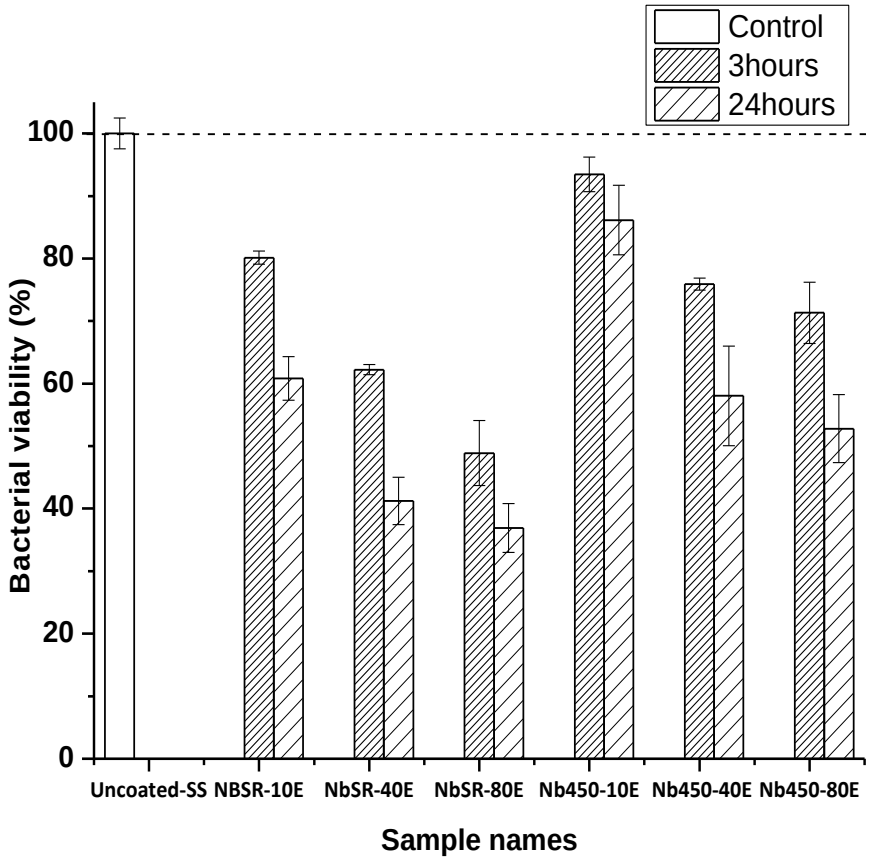

Figure 3. Bacterial viability of UC-SS and SR and IWIR coated niobium oxide after 3 and 24 hours of immersion in an *S.aureus* bacterial culture.

Figure 4 compared the representative SEM images of UC-SS, NbSR-80E than Nb450-80E after 24 hours immersion in TSA broth. The SEM image showed dark colored patches over all the sample surfaces which at higher magnification revealed spherical shaped particles corresponding to *S.aureus*. From the SEM image it is evident that the dark patches are more prominently present on the surface of UC-SS than SR and IWRI coatings for both 3 and 24 hours. It was further observed that the bacterial cells tend to cluster together when present in abundance. Among SR coatings, the area covered by dark patches was comparatively larger for NbSR-10E surface than both NbSR-40E and NbSR-80E for both 3 and 24 hours.

The appearance of the dark patches on NbSR-80E was considerably reduced and the round particles were also not clustered together due to lower concentration of bacteria on it. Among IWRI coatings, the area covered by dark patches was comparatively larger for Nb450-10E surface than both Nb450-40E and Nb450-80E for both 3 and 24 hours. Additionally, light colored particles deposits were also observed on the sample surfaces. The area covered by dark patches in SEM for IWIR coatings containing 40 and 80mg/l erythromycin was nearly identical. The SEM images indicated that the appearance of dark patches significantly reduced after 24 hours than 3 hours.

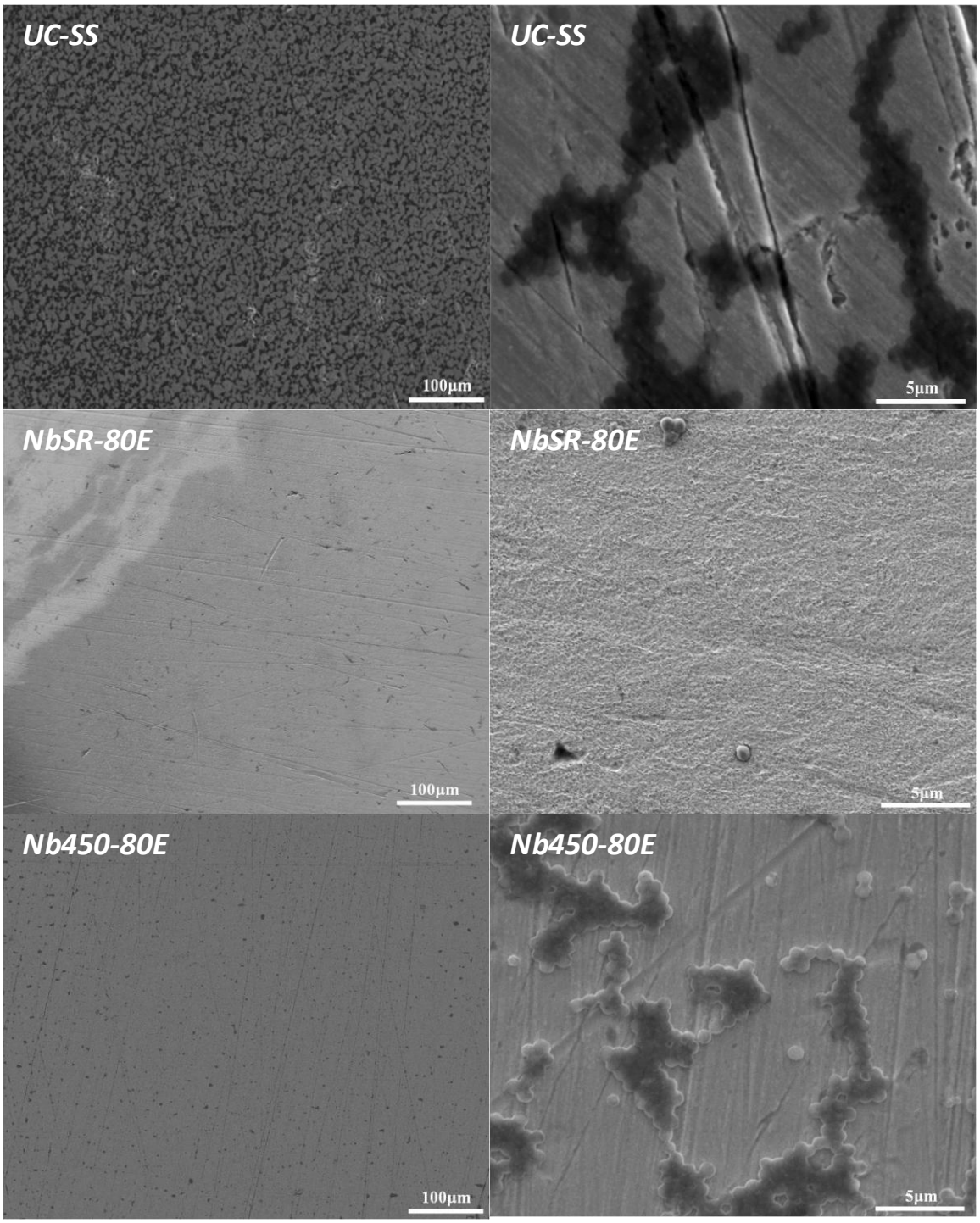

Figure 4. SEM images of a) UC-SS b) Nb450-80E and c) NbSR-80E after 24 hours in an *S.aureus* bacterial culture at 200x and 5kx.

4. Conclusions

Erythromycin in varying concentration was successfully incorporated into sol gel modified coatings using two different processing routes. The release of drug from coatings and performance against *S.aureus* was compared on the basis of processing routes, drug concentration and time of immersion.

We reported that, the addition of erythromycin up to 80mg/ml to the niobium based sol during SR processing did not cause it to precipitate. We also did not observe any cracks or pores on the coatings after erythromycin was embedded in the niobium oxide matrix. For IWRI-coatings, the coatings surface was spatially homogeneous with CaP deposition with Ca and P layer at the surface.

The release from SR-coatings containing 80mg/ml erythromycin was higher than MIC (0.5mg/ml) after 3 hours and was highest among the entire drug loaded coatings after 24 hours. This is in correlation with antibacterial study where coatings containing 80mg/l erythromycin showed maximum reduction in bacterial viability and bacterial adhesion on the surface after 24 hours. The release from IWRI-coatings containing 10mg/ml erythromycin was not detectable after 3 and 24 hours and release from 40 and 80mg/ml erythromycin was nearly identical. This is in correlation with the antibacterial study where IWIR coatings containing 40 and 80mg/l erythromycin showed nearly identical bactericidal activity. Additionally, coatings containing 40 and 80mg/l erythromycin showed enhanced bactericidal activity in comparison to those containing 10mg/l erythromycin.

For both SR and IWIR-coatings the concentration of erythromycin released increased with time of immersion and correspondingly the antibacterial properties were higher after 24 hours.

REFERENCES

1. V. Antoci, C.S. Adams, J. Parvizi, H.M. Davidson, R.J. Composto, T.A. Freeman, E. Wickstrom, P. Ducheyne, D. Jungkind, and I.M. Shapiro, "The inhibition of Staphylococcus epidermidis biofilm formation by vancomycin-modified titanium alloy and implications for the treatment of periprosthetic infection," *Biomaterials*, **29** [35] 4684-90 (2008).

2. H. Qu, C. Knabe, M. Burke, S. Radin, J. Garino, T. Schaer, and P. Ducheyne, "Bactericidal micron-thin sol-gel films prevent pin tract and periprosthetic infection," *Military medicine*, **179** [8S] 29-33 (2014).

3. P. Wu and D.W. Grainger, "Drug/device combinations for local drug therapies and infection prophylaxis," *Biomaterials,* **27** [11] 2450-67 (2006).

4. J.A. Jennings, D.P. Carpenter, K.S. Troxel, K.E. Beenken, M.S. Smeltzer, H.S. Courtney, and W.O. Haggard, "Novel antibiotic-loaded point-of-care implant coating inhibits biofilm," *Clin. Orthop. Relat. Res.*, **473** [7] 2270-82 (2015).

5. S. Radin, J.T. Campbell, P. Ducheyne, and J.M. Cuckler, "Calcium phosphate ceramic coatings as carriers of vancomycin," *Biomaterials,* **18** [11] 777-82 (1997).

6. S. Bhattacharyya, A. Agrawal, C. Knabe, and P. Ducheyne, "Sol–gel silica controlled release thin films for the inhibition of methicillin-resistant Staphylococcus aureus," *Biomaterials,* **35** [1] 509-17 (2014).

7. S. Radin and P. Ducheyne, "Controlled release of vancomycin from thin sol–gel films on titanium alloy fracture plate material," *Biomaterials,* **28** [9] 1721-9 (2007).

8. E.P. Avés, G.F. Estévez, M.S. Sader, J.C.G. Sierra, J.C.L. Yurell, I.N. Bastos, and G.D.A. Soares, "Hydroxyapatite coating by sol–gel on Ti–6Al–4V alloy as drug carrier," *J. Mater.Sci.: Mater. Med.*, **20** [2] 543-7 (2009).

9. S. Radin, T. Chen, and P. Ducheyne, "The controlled release of drugs from emulsified, sol gel processed silica microspheres," *Biomaterials,* **30** [5] 850-8 (2009).

10. W. Aughenbaugh, S. Radin, and P. Ducheyne, "Silica sol- gel for the controlled release of antibiotics. II. The effect of synthesis parameters on the in vitro release kinetics of vancomycin," *J. biomed. mater. res,* **57** [3] 321-6 (2001).

11. H. Böttcher, C. Jagota, J. Trepte, K.-H. Kallies, and H. Haufe, "Sol–gel composite films with controlled release of biocides," *J. controlled release,* **60** [1] 57-65 (1999).

12. E. Ghedini, M. Signoretto, F. Pinna, V. Crocellà, L. Bertinetti, and G. Cerrato, "Controlled release of metoprolol tartrate from nanoporous silica matrices," *Microporous and Mesoporous Mater,* **132** [1] 258-67 (2010).

13. Z. Wu, Y. Jiang, T. Kim, and K. Lee, "Effects of surface coating on the controlled release of vitamin B 1 from mesoporous silica tablets," *J controlled release,* **119** [2] 215-21 (2007).

14. M. Signoretto, E. Ghedini, V. Nichele, F. Pinna, V. Crocellà, and G. Cerrato, "Effect of textural properties on the drug delivery behaviour of nanoporous TiO 2 matrices," *Microporous and Mesoporous Materials,* **139** [1] 189-96 (2011).

15. W. Zhang, Y. Chen, S. Yu, S. Chen, and Y. Yin, "Preparation and antibacterial behavior of Fe 3+-doped nanostructured TiO 2 thin films," *Thin Solid Films,* **516** [15] 4690-4 (2008).

16. M. Stigter, J. Bezemer, K. De Groot, and P. Layrolle, "Incorporation of different antibiotics into carbonated hydroxyapatite coatings on titanium implants, release and antibiotic efficacy," *J controlled release,* **99** [1] 127-37 (2004).

17. R. Wankhade, S. Bhalerao, S. Panchory, A. Pundir, and R. Pradhan, "Analysis of erythromycin and benzoyl peroxide in combined dosage form by UV-visible spectrophotometry," *Int J Pharm Pharm Sci,* **4** [4] 527-31 (2012).

18. A. Bagchi, P. Mukherjee, and A. Raha, "DEVELOPMENT AND VALIDATION OF UV SPECTROPHOTOMETRIC METHOD FOR ESTIMATION OF ERYTHROMYCIN IN BULK DRUG AND PHARMACEUTICAL FORMULATION."*Int. J Recent Adv. Pharma. Res,* **5** [3] 71-76 (2015)

19. B.A. Akgun, A.W. Wren, C. Durucan, M.R. Towler, and N.P. Mellott, "Sol–gel derived silver-incorporated titania thin films on glass: bactericidal and photocatalytic activity," *J Sol-Gel Sci. Technolo,* **59** [2] 228-38 (2011).

20. D. Pradhan, A. Wren, S. Misture, and N. Mellott, "Investigating the structure and biocompatibility of niobium and titanium oxides as coatings for orthopedic metallic implants," *Mater. Sci. Eng.: C,* **58** 918-26 (2016).

21. S. Salmon, J. Watts, F.M. Aarestrup, J. Pankey, and R. Yancey, "Minimum inhibitory concentrations for selected antimicrobial agents against organisms isolated from the mammary glands of dairy heifers in New Zealand and Denmark," *J. dairy science,* **81** [2] 570-8 (1998).

22. M. Stigter, K. De Groot, and P. Layrolle, "Incorporation of tobramycin into biomimetic hydroxyapatite coating on titanium," *Biomaterials,* **23** [20] 4143-53 (2002).

CONCLUSION

We have successfully developed sub-micron, crack-free, and spatially homogeneous amorphous niobium oxide and silicon oxide coatings on 316L via sol-gel processing. These coatings improved the biocompatibility of 316L stainless steel by formation of bone-like apatite along with enhanced osteoblast viability and adhesion on the surface. We show that both the adhesion to and viability of osteoblast cells is higher for the niobium oxide coated 316L than the silicon oxide coated 316L.

The LPR values in water for UC-SS were significantly higher than other two media. The LPR value in SBF and SGF for UC-SS were nearly same. The LPR values in water for Nb-SS were highest in water followed by SBF and then SGF. The presence of Ca and P layer restricted Fe dissolution in SBF while presence of Cl^- ions and inherent porosity allowed easy interaction of SGF with substrate underneath the coating. The LPR values in Si-SS were highest for water but due to cracking and peeling of coatings the Rp values were nearly same for SBF and SGF.

Niobium oxide was selected as a carrier for erythromycin based on its inherent porosity and results from biocompatibility and corrosion studies. Erythromycin in varying concentration was successfully incorporated into sol gel modified niobium oxide coatings using two different processing routes (SR and IWRI-coatings). The release of drug from coatings and performance against *S.aureus* was compared on the basis of processing routes, drug concentration and time of immersion. The release from SR-coatings containing 80mg/ml erythromycin was higher than MIC (0.5mg/ml) after 3 hours. After 24 hours, the release from SR-coatings containing 80mg/ml antibacterial properties was highest along with maximum reduction in bacterial viability and bacterial adhesion on the surface. The release from IWRI-coatings containing 10mg/ml erythromycin was not detectable and consequently the bacterial adhesion and viability were not optimistic. The release from 40 and 80mg/ml erythromycin was nearly identical which is in correlation with their identical bactericidal activity. For both SR and IWIR-coatings the concentration of erythromycin released increased with time of immersion and correspondingly the antibacterial properties were higher after 24 hours.